Centro de Investigación Científica y de Educación

Superior de Ensenada, Baja California

Programa de Posgrado en Ciencias en Óptica

Studies of fluorophores in a fluorescence microscopy system

Tesis

para cubrir parcialmente los requisitos necesarios para obtener el grado de

Maestro en Ciencias

Presenta:

Beatriz Alina Juárez Álvarez

Ensenada, Baja California, México

2015

Tesis defendida por

Beatriz Alina Juárez Álvarez

y aprobada por el Comité

Dr. Kevin Arthur O'Donnell
Director del Comité

Dr. Veneranda Guadalupe Chávez Garcés

Dr. Eugenio Rafael Méndez Méndez

Dr. Héctor Manuel Escamilla Taylor

Dr. Helmut Maske Rubach

Autoridades

Dr. Pedro Negrete Regagnon
Coordinador del Posgrado en Óptica

Dra. Rufina Hernández Martínez
Directora de Estudios de Posgrado

Resumen de la tesis que presenta Beatriz Alina Juárez Álvarez como requisito parcial para la obtención del grado de Maestro en Ciencias en Óptica.

Estudios de fluoróforos en un sistema de microscopía de fluorescencia

Resumen aprobado por:

Dr. Kevin Arthur O'Donnell
Director de tesis

El propósito de este trabajo fue investigar los parámetros teóricos y experimentales involucrados al hacer mediciones de fluorescencia inducida en muestras de fluoróforos en la escala microscópica. El fluoróforo utilizado fue Rodamina B con metanol como solvente. Se hizo una revisión bibliográfica de los fundamentos de la fluorescencia, los parámetros involucrados, y las características del fluoróforo utilizado. La distribución espacial de la intensidad cerca del foco de un objetivo de microscopio con abertura numérica baja iluminado con un haz Gaussiano truncado fue calculada utilizando el método descrito por Horvath y Bor (2003). Posteriormente, se diseñó y construyó un sistema de microscopía de fluorescencia con dos posibles geometrías (epifluorescencia y geometría 4pi). Esto permitió investigar la influencia de parámetros relacionados con la muestra, como son la concentración y el espesor. También permitió estudiar los efectos de los parámetros del sistema, tales como la longitud de onda de excitación, la posición de enfoque del objetivo de microscopio, el uso de fuentes de excitación continua o pulsada, y la geometría del sistema de colección. Entre los resultados obtenidos, el uso de la geometría 4pi y la cuidadosa selección de los parámetros estudiados permitió señales observables de fluorescencia usando potencia de excitación incidente en la muestra de tan solo 0.5 nW. Información sobre la intensidad de saturación se extrajo de los datos obtenidos con el láser pulsado, lo cual permitió determinar la sección transversal de excitación del fluoróforo.

Palabras Clave: **fluorescencia, Rodamina B, microscopía**

Abstract of the thesis presented by Beatriz Alina Juárez Álvarez as a partial requirement to obtain the Master of Science degree in Optics.

Studies of fluorophores in a fluorescence microscopy system

Abstract approved by:

Dr. Kevin Arthur O'Donnell
Thesis advisor

The purpose of this work was to investigate the theoretical and experimental parameters involved in fluorescence induced in liquid fluorophore samples at a microscopic scale. The fluorophore used was Rhodamine B with methanol as the solvent. A bibliographical review of the fundamentals of fluorescence, the parameters involved, and the characteristics of the fluorophore used was done. The spatial distribution of the intensity near focus for a low N.A. microscope objective illuminated with a truncated Gaussian beam was calculated using the approach of Horvath and Bor (2003). Then, a fluorescence microscopy system with two possible geometries (epifluorescence and 4pi geometry) was designed and constructed. It allowed for the effects of parameters related to the sample, such as concentration and thickness, to be investigated. It also permitted study of the effects of system parameters, such as the wavelength of excitation, focusing position of the microscope objective, use of continuous or pulsed excitation, and geometry of the collection system. Among the results obtained, the use of the 4pi geometry and careful selection of the studied parameters allowed for observable signals with excitation power incident on the sample as little as 0.5 nW. Information for intensity saturation was extracted from the pulsed excitation source data, which allowed for determination of the absorption cross-section of the fluorophore.

Keywords: **fluorescence, Rhodamine B, microscopy**

Dedication

To my parents.

Acknowledgements

First of all, I would like to thank my family for their unconditional love and support. To my Dad for always encouraging me to try my best and to never give up. To my Mom for her selflessness and dedication to our family. To my darling Abuelita, for her blessings every morning, for keeping me in her prayers every night, and for all our shared memories. To Romy for being the 'best sister ever' and for motivating me during stressful times. And to Joctan, my partner, for swimming through life with me.

I still cannot believe how fortunate I am, for having had the opportunity to witness how hard the people in Professor O'Donnell's group work. Please know that I have a deep admiration for you, and that I will always be grateful for all the help and support you have given me. To Dr. Kevin O'Donnell for giving me the opportunity and accepting me as a student, for your insights, and for patiently explaining things to me. To Dr. Veneranda Garcés, for going beyond being a member of the committee and taking the role of an unofficial advisor. To Daniel Jiménez, for the pep-talks and for providing the documentation to set up the GPIB-USB interface needed to record data.

To the other members of the committee, for fitting time in their busy schedules for me, and for all the helpful questions and comments that enabled me to improve this thesis. Thank you Dr. Eugenio Méndez and thank you Dr. Héctor Escamilla, for formaly introducing me to the wonders of optics in the first place, and for being such an inspiration in my early academic career. Thank you Dr. Helmut Maske, for sending me interesting articles, and lending me a high accuracy scale for the preparation of the samples.

I would also like to thank Consejo Nacional de Ciencia y Tecnología (CONACyT) for the monetary support they gave me while undertaking these studies. A huge thanks to Centro de Investigación Científica y de Educación Superior de Ensenada (CICESE) and all the people within it, for providing a simulating environment, and for being so helpful every step of the way.

And lastly, I would like to express my eternal gratefulness to God, for always guiding my path and giving me the strength to continue moving forward.

Table of contents

Page

List of figures

List of tables

Chapter 1. Introduction

In this project, experimental and theoretical studies of fluorescence phenomenon are performed. One of the main goals of this work, is to detect fluorescence using low excitation power. For this reason, a fluorescence microscopy system has been built. In the results obtained, the observation of fluorescene with excitation powers as low as 0.5 nW is quite notable. The fluorophore used throughout the studies is Rhodamine B disolved in methanol.

1.1 Fluorescence microscopy and fluorophores

Fluorescence is a process in which a molecule of a material that is being illuminated is taken to a higher energy state due to the absorption of one or more photons. After a time on the order of nanoseconds, it relaxes and goes back to its initial state, liberating a photon of longer wavelength.

The phenomenon of fluorescence was first incorporated into an optical microscope by O. Heimstedt and H. Lehmann in 1911 [ZEISS-Campus, 2015]. The technique has since been called fluorescence microscopy and it has now become one of the most important tools used in the life sciences.

By using fluorescence microscopy, studies of cell behavior and the visualization of cellular functions at the molecular level, such as detection and monitoring of specific proteins, nucleic acids and lipids in living or fixed cells, can be performed. Fluorescent probes can be used to examine physiological ion concentrations, pH values, viscosity, polarity, and even temperature [Valeur, 2001].

Fluorescence microscopy consists of using a microscope objective lens to tightly focus a beam of a specific wavelength into a small volume of a sample that has the ability to produce fluorescence. If the sample does not fluoresce on its own, compounds called fluorophores (that bind themselves to target microscopic structures) can be added to produce this effect [Spring and Davidson, 2015b]. The wavelength used is such that it excites the fluorophores.

Even though fluorescence microscopy has been in wide use for several decades, performing measurements with living cells using fluorescence is an area of active research. Two major issues have to be addressed: The control of the spatial-temporal distribution of the sample excitation, and the sample preparation.

Regarding sample preparation, the use of fluorophores to stain biological samples was initiated in the 1930s [Spring and Davidson, 2015b]. The number of fluorophores available for use has increased dramatically over the past decade, expanding the spectrum of possibilities, and improving properties like quantum yield and resistance to photobleaching [Lakowicz, 2007]. The selection of the fluorophore ultimately depends on the application, but some of the most common types used are fluorescein, rhodamine, GFP, and erythrosine; these molecules are small (20-100 atoms) and are available as liquid homogeneous media or soluble powder.

For excitation and collection, many techniques have been developed for fluorescence microscopy. The most common is epifluorescence microscopy, in which the excitation of the sample and collection of the fluorescent light is obtained from the same side by using the same microscope objective [Jensen, 2012].

1.2 Objectives

The purpose of this project is to investigate the theoretical and experimental parameters involved in the measurement of fluorescence occurring in an aqueous sample at the microscopic scale. Some specific objectives were:

- Design and construct an experimental fluorescence microscopy system.
- Study the influence that the distribution of the optical field applied to a sample has in the fluorescence measurements.
- Determine the optimum concentration and thickness of the sample to achieve a high efficiency.
- Find the system parameters that will enable low power excitation of observable levels of fluorescence.

1.3 Outline

The thesis is divided into five chapters. This first chapter has the purpose of serving as an introduction, by providing general information about fluorescence microscopy, and discussing the objectives of the project. Chapter 2 contains the theoretical material that is essential in understanding how to design the experimental system. The fundamentals of fluorescence, and details about the parameters involved in fluorescence measurements are presented. This chapter also contains numerical simulations of the excitation beam structure. Chapter 3 describes the experimental system that has been constructed. Description of the sample preparation and the fluorescence microscopy system are shown. The results obtained from the experiments are presented and discussed in Chapter 4. The conclusions derived from this work are given in Chapter 5.

Chapter 2. Theoretical Preliminaries

In this chapter, the theoretical preliminaries needed to better understand this thesis are presented. Section 2.1 is about optical microscopes, with the basics of microscopy being presented in Subsection 2.1.1, types of optical microscopes introduced in Subsection 2.1.2., and some interesting microscopy parameters being defined in Subsection 2.1.3. The fundamentals of the process leading to fluorescence are given in Section 2.2. Details about the parameters involved in fluorescence measurements with fluorophores, such as the quantum efficiency, absorption cross-section, concentration, collection efficiency, excitation volume, and temporal profile of the excitation beam, can be found in Section 2.3. Finally, some simulations of the spatial distribution of the excitation beam are shown in Section 2.4.

2.1 Optical Microscopy

Microscopes are instruments that have the purpose of making visible small objects or details that are not distinguishable with the naked eye. The optical microscope uses light and lenses to produce a magnified image of an object. A positive lens used in conjunction with the eye to produce a magnified image of an object can be considered to be the simplest kind of microscope [Abramowitz, 2003]. Most microscopes used today are compound, which means that they use more than one lens. Traditionally, the useful magnification that could be achieved was limited by the diffraction, but more recently, new techniques have emerged that increase the optical resolution beyond the wavelength limit [Hell and Wichmann, 1994].

2.1.1 Introduction to optical microscopes

The invention of the compound microscope is attributed to a spectacle maker called Zacharias Janssen, and is believed to have been developed in 1590 [Hecht, 2002]. Figure 1 shows the schematic of a compound microscope. This type of microscope magnifies in two steps. First, the objective lens, if the object is located in a position that is to the left of the focal point f_o, produces an inverted magnified real image of the object. This magnified image is known as the intermediate image, and the eyepiece is positioned so that

the front focal plane of the eyepiece (defined by f_e) will lie in the same plane. The eyepiece then produces a virtual image in the observer's eye. Objective lenses are nowadays actually composed of many lenses cemented together that act as one, to correct optical aberrations. Eyepieces have lower magnifications than objectives, but are also composed of more than one lens. The optical tube length is defined as the distance between f'_o and the plane where the intermediate image is formed. Even though the tube length was standardized to 160 mm by the Royal Microscopical Society, the need of inserting components after the objective without affecting the image lead to the development of a kind of compound microscope that works slightly differently and is called infinity corrected. In this kind of microscope, the object is placed at f_o, and the light comes out collimated after the objective until an additional lens (called tube lens) is used to form the intermediate image. After that, the eyepiece can be used the same as with the other fixed tube length type.

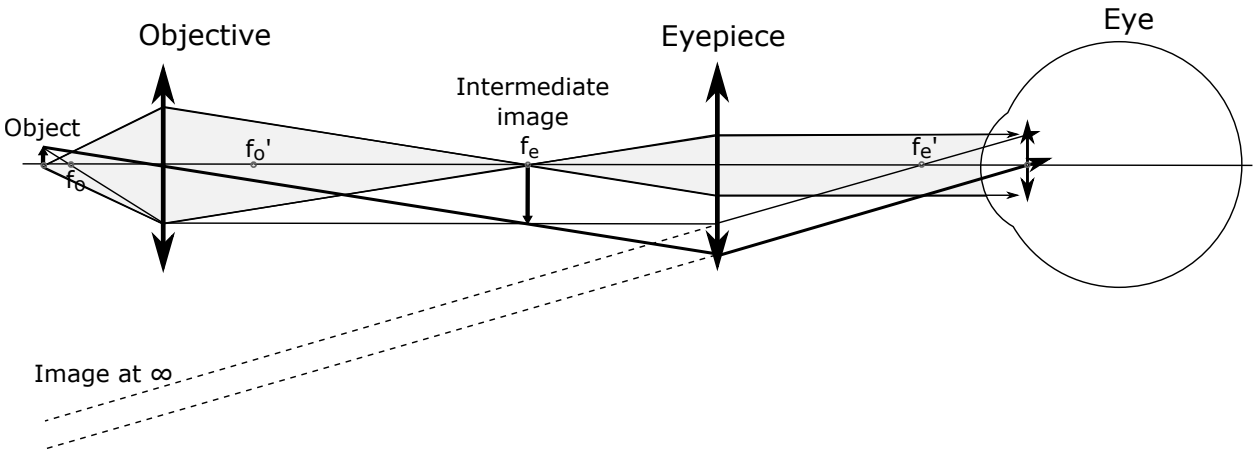

Figure 1: Schematic of a compound microscope.

Modern microscopes have optics that correct for a variety of aberrations, and are also designed to accommodate other optical and mechanical components [Sluder and Wolf, 2003]. Consequently, most microscopes currently used for research have multiple light paths and relay lenses that project the intermediate image to various positions.

Instead of using the eye to examine the sample through the microscope, other instruments with photo-detecting surfaces may be employed in order to capture and record information. When imaging is required, using a digital camera (with photo-detecting surfaces based on CCD or CMOS technology) allows the ability to enhance features, extract information, and do image processing [Spring *et al.*, 2015]. The detecting surface must

be positioned at a location in which the microscope projects an intermediate image plane. A less common way is by using an additional lens to project the image onto the sensor [Sluder and Wolf, 2003].

2.1.2 Types of modern optical microscopes

Most microscopes used nowadays are compound, but there are many different configurations that can be used. The selection depends on the kind of sample that needs to be observed, and on what technique is to be employed. In microscopes that have a vertical geometry, inverted microscopes are preferred when working with biological samples that tend to set to the bottom of the microscope slide. For fluorescence microscopy, as mentioned in Section 1.1, the most common technique is epifluorescence microscopy, in which the excitation of the sample and collection of the fluorescent light is done with the same microscope objective. The element that allows such a configuration is a dichroic filter, which reflects the excitation light and transmits the fluorescence. Another technique is confocal microscopy which, by using a pinhole to block light that does not come from the focal plane, limits the collection to a small volume, which increases the resolution. The 4pi microscopy technique also helps increase the resolution and double the collection. It consists of using two microscope objectives, one positioned above and one below the sample, to simultaneously illuminate and collect from both sides.

For the purposes of this thesis, from now on, the configuration in which two identical microscope objectives are positioned just as in the 4pi microscopy technique will be called 4pi geometry. Figure 2 illustrates a basic system configuration schematic for excitation and collection with epifluorescence and 4pi geometry.

2.1.3 Interesting parameters

According to Abramowitz (2003), the three most important functions of an optical microscope are to produce a magnified image of the object, resolve details in the image, and render the details visible to the imaging device. The essential parameters to be aware of are then the magnification, the resolution, and the contrast of the imaging device.

The magnification M is defined as the ratio between the size of the image and the size

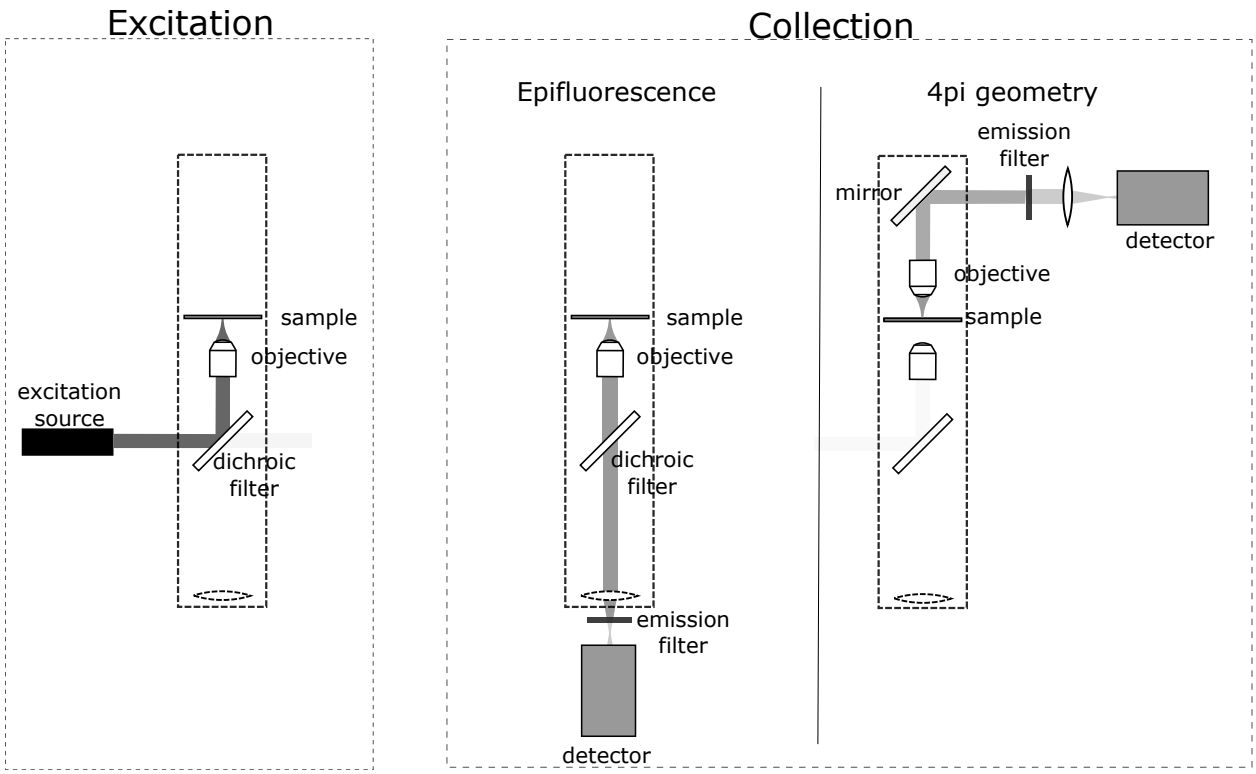

Figure 2: Excitation and collection for epifluorescence and 4pi geometries.

of the original object

$$M = \frac{h_i}{h_o}, \tag{1}$$

where h_i is the image height, and h_o is the object height. For compound microscopes in which the eyepiece is used in conjunction with the objective, the magnification is obtained by multiplying the magnification that each of the lenses produces individually:

$$M = M_o M_e, \tag{2}$$

where 'o' refers to objective and 'e' refers to the eyepiece.

Common values for the magnification of microscope objectives are 4x, 10x, 20x, 40x, 60x, 80x, and 100x [Spring and Davidson, 2015b]. The magnification of a microscope objective depends on its focal length f and the tube length d_{tube} as

$$M = \frac{d_{tube}}{f}. \tag{3}$$

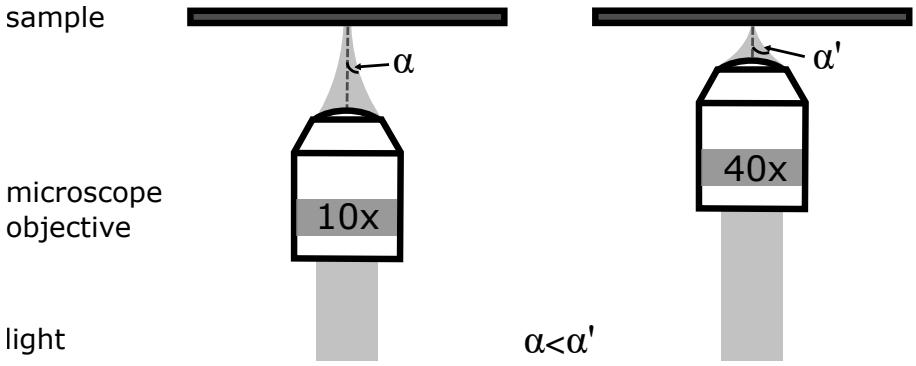

Figure 3: Illustration of the half angular aperture of objectives with different magnification.

The numerical aperture (N.A.), is defined as

$$N.A. = n\sin(\alpha), \tag{4}$$

where n is the index of refraction of the medium between the front of the objective and the sample, and α is the half angular aperture of the objective, as seen in Fig. 3. The numerical aperture is related to the focal length of the lens through

$$f = \frac{a}{\tan\left[\sin^{-1}\left(N.A./n\right)\right]}, \tag{5}$$

where a is the back aperture radius of the lens.

Resolution in an optical microscope is defined as the shortest distance between two points on the sample that can be distinguished as separate entities. The limit of resolution is given by the radius of the Airy disk r_0,

$$r_0 = 0.61\frac{\lambda}{N.A.}, \tag{6}$$

where λ is the wavelength (or average wavelength in case of white light illumination) that is being used.

Another useful parameter when obtaining images with a microscope is the field of view. This is the actual size of the object field that is seen in the image. It is usually determined by either the eyepiece when viewing directly, or by the sensor size when using a camera. A straightforward way to measure it is by imaging an object of known dimensions, such

as a graduated reticle, and using it as reference to calibrate the size of the field. A higher magnification usually implies a smaller field of view.

Depth of field and depth of focus are sometimes used interchangeably, but they are not the same. Depth of field refers to the distance above and below the focal plane in which an object still remains acceptably focused [Abramowitz, 2003]. Depth of focus is similar, but instead of referring to object space, it refers to image space. The depth of field is given by

$$\Delta z = \frac{n\lambda}{N.A.^2}, \tag{7}$$

with n corresponding to the refractive index of the medium between the sample and the objective lens, λ being the wavelength used for illumination, and with N.A. representing the numerical aperture of the objective lens. In digital microscopy, a reduced depth of field can help produce very sharp and thin optical sections of the specimen [Spring and Davidson, 2015a].

2.2 Fundamentals of Fluorescence

Fluorescence is a process by which a molecule that has absorbed a photon of certain wavelength, dissipates its energy in a radiative form by spontaneously emitting a photon of longer wavelength. Molecules which exhibit such a property are called fluorophores. A Jablonski diagram (see Fig. 4) is helpful to describe the process by which fluorescence occurs. In this diagram, the electronic energy levels of a molecule are displayed, the higher the position, the higher the energy. For this particular figure, each stack of horizontal lines represent an electronic energy state (labeled as S_0, S_1, S_2, ...), while each of the lines in the stack represents a vibrational energy level (labeled as V_0,V_1,V_2,...). It should be noted that because of the large number of possible vibrational energy levels, only a few are drawn. Also for simplicity, the energy states above the second excited singlet state (S_2) are not drawn. The separation between states diminishes at higher levels, eventually leading to a continuum. The separation of the levels and the probability of transitions are characteristic of the particular fluorophore.

Under equilibrium conditions, most of the molecules are in a low vibrational level of the ground state, as given by the Boltzmann distribution. Of course, increasing temperature

increases the probability of the molecule being in a higher level. When a photon hits a fluorophore, it interacts with the electrons of the molecule and transfers its energy to them. This process is known as absorption, and it takes the fluorophore from the ground state S_0 to one of the excited singlet states (S_1,S_2,S_3,...), in a matter of femtoseconds [Valeur, 2001]. Absorption of light energy can only happen in discrete amounts (quanta), which implies that if the associated energy of the photon does not match the energy between the states, then it cannot occur. The energy of a photon is given by

$$E = h\nu, \tag{8}$$

where h is Planck's constant and ν is the frequency of the photon. The frequency is related to the wavelength of the photon through,

$$\nu = \frac{c}{\lambda}, \tag{9}$$

where c is the speed of light and λ is the wavelength of the photon.

With the fluorophore in an excited state, there are de-excitation processes that can occur, which can be either radiative or non-radiative. Internal conversion and vibrational relaxation are two non-radiative processes that, because they are very fast (picoseconds), are the ones that usually follow absorption. If it happens from S_2 (or higher) to S_1, as in the middle set of arrows of Fig. 4, it is called internal conversion. If the dissipation occurs within the same electronic state, like in the leftmost set of arrows of Fig. 4, it is known as vibrational relaxation. For fluorescence to occur after absorption, the excited molecule first relaxes to the lowest vibrational level of the first excited singlet state S_1. From there, after a time of the order of nanoseconds, the excited molecule releases its energy, going from S_1 to one of the vibrational levels of the ground state S_0 with the spontaneous emission of a photon.

The energy of the emitted photon is less than the total absorbed energy, because some of it is lost from internal conversion. This means that the emission spectrum is shifted towards longer wavelengths in comparison with the excitation spectrum. The difference in the central wavelength between the excitation light and the emitted light is known as

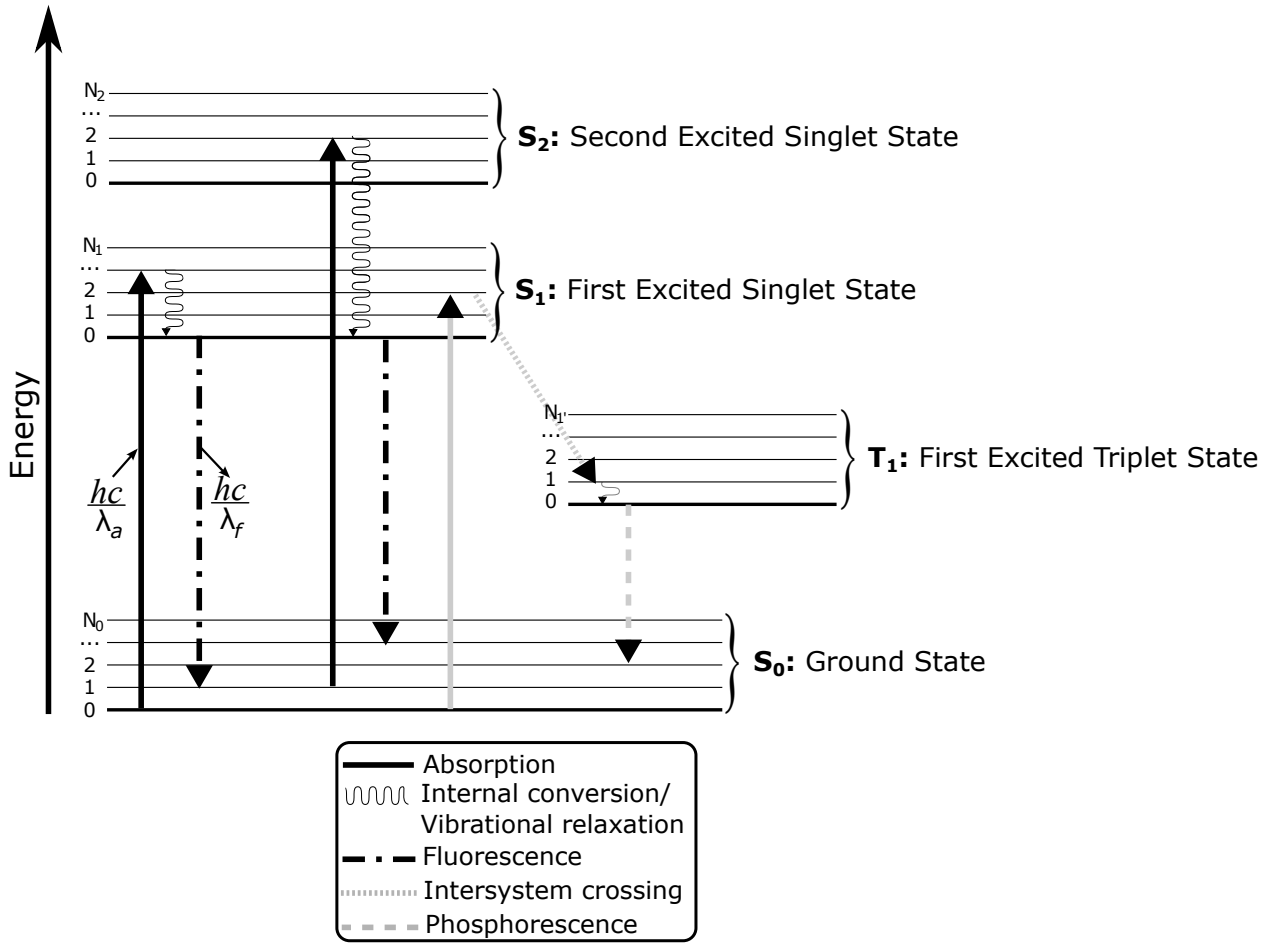

Figure 4: Jablonski diagram showing the molecular energy transitions leading to fluorescence emission and other relaxation processes.

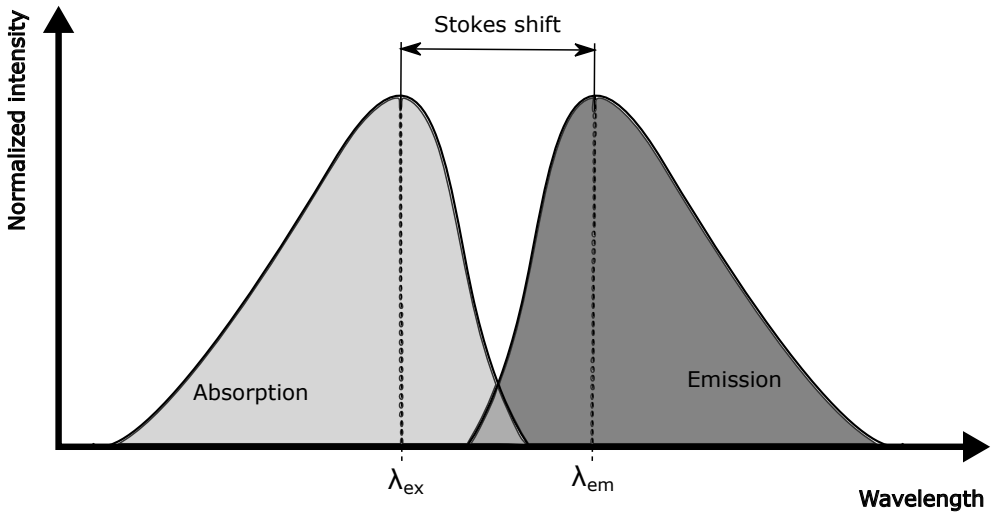

Figure 5: Typical absorption and emission spectra, showing how the Stokes shift is defined.

the Stokes Shift (see Fig. 5). Thanks to this shift between the excitation and emission wavelengths (marked as λ_{ex} and λ_{em} respectively), it is possible, with the use of filters, to separate the excitation light from the emitted light.

It should be mentioned that there is another radiative process that can occur after absorption of light called phosphorescence. This is a much slower process (of the order of seconds) that can happen if, as illustrated in Fig. 4, the molecule goes from the single excited state to a triplet excited state through a process called intersystem crossing. The occurrence of phosphorescence in most fluorophores is a more unlikely process than fluorescence because intersystem crossing rarely happens. According to Boni *et al.* (2001), for Rhodamine B dissolved in methanol (as used in this thesis), the population transfer to the triplet state is negligible. Thus, even though there are numerous relaxation processes that can occur after absorption, it is certain that the emitted photons are due to fluorescence.

To explain the effects of using linearly polarized light as excitation, it is good to know that, due to the chemical structure of the fluorophore, each molecule has a transition moment that makes it act like a dipole. For a homogeneous fluorophore sample, the molecules are randomly oriented. The molecules that have a transition moment oriented in a direction close to that of the electric vector of the incident beam are preferentially excited [Valeur, 2001]. This is known as photoselection, and it produces an anisotropic distribution of the excited fluorophores. Then, even though the emitted fluorescence would also be anisotropic, if the fluorophore has enough time to rotate or move before emission, then a loss of the anisotropy may occur.

2.3 Parameters involved in fluorescence measurements using fluorophores

Because detection of fluorescence is to be achieved even with low excitation power, it is essential to consider the parameters involved in fluorescence emission and its detection. A useful model, generalized for multiphoton excitation, was developed by Xu and Webb in 1996. According to these authors, the number of photons absorbed by a fluorophore

sample per unit of time can be expressed as

$$N_{abs}(t) = \int_V d\vec{r} C(\vec{r}, t) \sigma_n I^n(\vec{r}, t), \tag{10}$$

where n is the number of photons needed (in the case of linear absorption, $n = 1$), σ_n is the absorption cross-section, $C(\vec{r}, t)$ is the concentration, and $I(\vec{r}, t)$ is the photon flux (intensity or irradiance) and the integral is performed over the illuminated sample volume.

The number of fluorescence photons collected per unit time is related to N_{abs} through the expression

$$F(t) = \frac{1}{n} \phi \eta N_{abs}(t), \tag{11}$$

where ϕ is the collection efficiency of the system, and η is the fluorescence quantum efficiency.

If the sample is homogeneous and if no photobleaching or saturation occurs, then the concentration does not depend on time or spatial coordinates and $C(\vec{r}, t)$ can be expressed as C. Furthermore, if the irradiance's spatial and temporal dependence can be separated as

$$I(\vec{r}, t) = S(\vec{r}) I_0(t), \tag{12}$$

where $S(\vec{r})$ is a dimensionless spatial distribution function, and $I_0(t)$ is the temporal dependent intensity at the geometric focal point. Then, Eq. (10) can be written as

$$N_{abs}(t) = C \sigma_n I_0^n(t) \int_V d\vec{r} S^n(\vec{r}). \tag{13}$$

A detector measures a temporal average so, combining Eqs. (11) and (13) and taking the time average, the measured fluorescence photon flux $\langle F(t) \rangle$ is

$$\langle F(t) \rangle = \frac{1}{n} \phi \eta \sigma_n C \left\langle I_o^n(t) \right\rangle \int_V d\vec{r} S^n(\vec{r}). \tag{14}$$

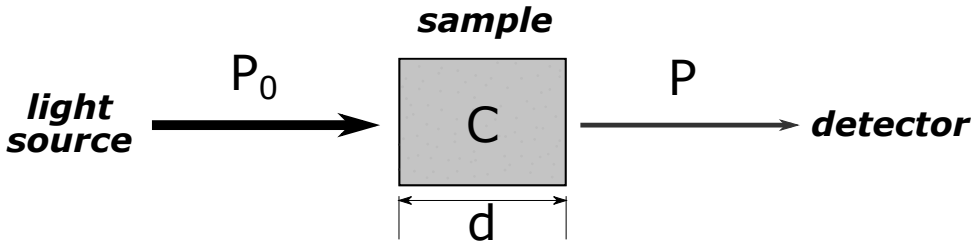

Figure 6: Schematic for obtaining the molar extinction coefficient with the Beer-Lambert law.

In the case of linear absorption ($n = 1$), Eq. (14) can be written as

$$\langle F(t)\rangle = \phi\eta\sigma C \langle I_o(t)\rangle \int_V d\vec{r} S(\vec{r}). \tag{15}$$

2.3.1 Absorption cross-section

The absorption cross-section is defined as the ratio between the radiant power absorbed by the particle to the radiant power incident on the particle. It gives a measure of how likely light incident on the particle will get absorbed.

The absorption cross-section σ has a relationship with the molar extinction coefficient ϵ [Lakowicz, 2007]

$$\sigma = 3.82 \times 10^{-21}\epsilon \text{ (in cm}^2\text{)}. \tag{16}$$

The molar extinction coefficient can be found by using the Beer-Lambert law, which in case of constant illumination area (such as a collimated beam) is expressed as

$$Log\left(\frac{P_0}{P}\right) = \epsilon C d, \tag{17}$$

where P_0 is the power measured before the sample, P is the power measured after the sample, C is the concentration of the solution, and d is the thickness of the solution layer. Figure 6 shows a schematic for the measurement of the molar extinction coefficient obtained through the Beer-Lambert law. Solving for ϵ in Eq. (17) and substituting into Eq. (16), the absorption cross-section is

$$\sigma = 3.82 \times 10^{-21}\frac{Log\,(P_0/P)}{Cd} \text{ (in cm}^{-2}\text{)}. \tag{18}$$

2.3.2 Fluorescence quantum efficiency

The quantum efficiency of a fluorophore, also known as the quantum yield, is a measure of the probability that an absorbed photon will produce fluorescence. It is defined as the ratio between the fluorescence emission rate to the absorption rate. Its value depends on the fluorophore, and it lies within the range from 0 to almost 1. The value of the fluorescence quantum efficiency can be influenced by other parameters such as the concentration, the polarity and viscosity of the solvent, and the temperature [Valeur, 2001]. For the fluorophore Rhodamine B, the quantum efficiency can range from 0.1 to 0.9 depending on the concentration and solvent used [Bindhu and Harilal, 2001].

2.3.3 Collection efficiency

When performing measurements of fluorescence, not all of the generated fluorescence photons can be collected. The amount of photons that reach the detector depends mostly on the angle of acceptance of the collection objective, but the transmittance of all the optical elements in the collection path also play a part [Xu and Webb, 2002] . Even if the transmission of all the elements in the optical path were an idealized 100%, and even if a high 1.4 N.A. were used to maximize the solid angle through which the instrument collects fluorescence, only about 30% of the fluorescence could be sent to the detector due to the collection cone [Spring and Davidson, 2015b].

2.3.4 Concentration

The number of fluorescence photons detected depends on the number of photons absorbed, which in turn depends on how many fluorophore molecules are contained within the volume illuminated with the excitation beam. As was apparent in Eq. (10), the value for the concentration may be space and time dependent. For a homogeneous sample (such as a fluorophore solution), the concentration can be considered as constant, with the exception of situations in which photobleaching and saturation occur. In chemistry, the concentration of a solution is defined as the amount of solute in a solvent. The most common way of expressing it is with molar concentration, which gives the amount of moles of solute in the solution volume, and is specified in mols per liter (mol/L).

2.3.5 Temporal profile of excitation source

The amount of fluorescence measured depends on the excitation power and how that power is supplied in time to the fluorophore sample. A laser is termed as being continuous wave (CW) if it produces a continuous output beam. There can be slight variations in the output power (typicaly 1-3%), but it is essentially constant. The counterpart of a CW laser is a pulsed one, which emits pulses with a repetition rate. Figure 7 shows a schematic of the power dependence on time for the two types of sources. It should be noted that the square shape of the pulses of Fig. 7 are an idealization.

Though the average excitation power can be the same for both types of sources, the peak power provided by a pulsed laser can be much higher. The peak power is defined as

$$P_{peak} = \frac{P_{average}}{\Delta t f}, \tag{19}$$

where $P_{average}$ is the average power, Δt is the pulse width, and f is the frequency of repetition (which can also be defined in terms of the period T as$f = 1/T$). For example, in the case of a pulsed laser with $\Delta t = 800$ ps and $f = 20$ kHz, the peak power is 62,500 times higher than the average power. This means that if excitation with the same average power is compared for the two types of sources, many more photons will be sent with the pulsed laser into the sample during the duration of the pulse. If there is a finite number of fluorophore molecules to be excited, and an excited molecule must return to the ground state before it can absorb again, excitation with a pulsed laser may lead to depletion of the ground state. This produces a saturation of the fluorescence, in which case Eq. (15) does not hold.

2.3.6 Spatial distribution of the intensity

The way the excitation light focuses into a fluorophore sample determines the volume of excitation which, in conjunction with the concentration, determines the number of fluorophore molecules being illuminated.

A common choice is to use a focused Gaussian laser beam to excite the sample. Some of the important parameters in a Gaussian beam are labeled in the schematic shown in

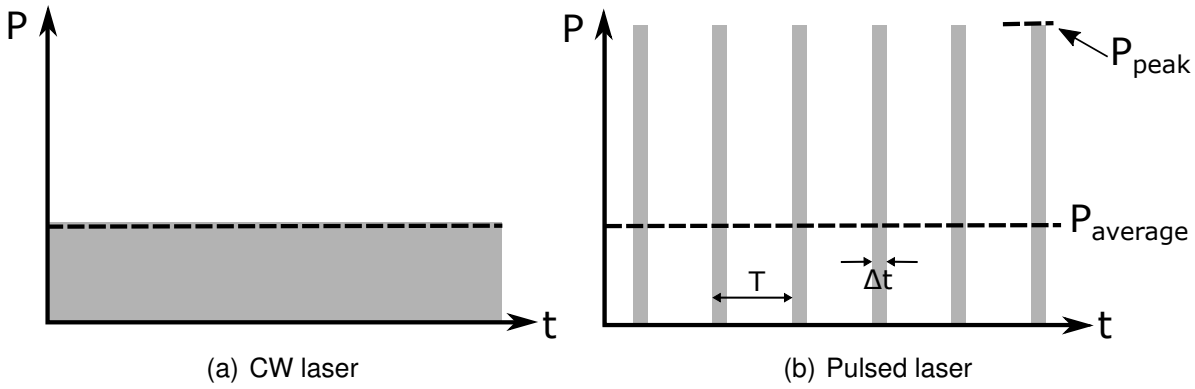

(a) CW laser (b) Pulsed laser

Figure 7: Comparison of laser output power for (a) continuous (CW) and (b) pulsed sources.

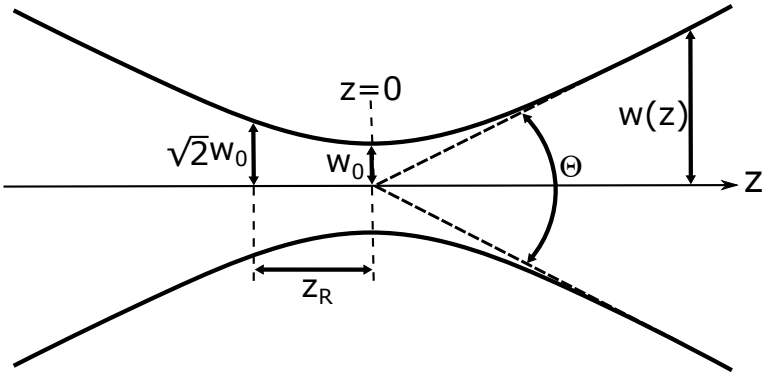

Figure 8: Gaussian beam parameters.

Fig. 8 [Saleh and Teich, 2007]. The parameter w_0 represents the beam waist radius, with $2w_0$ being known as the spot size. The plane of the beam waist is considered as $z = 0$. The beam width at a distance z from the beam waist is represented by $w(z)$. The Rayleigh range z_R is the axial distance from $z = 0$ to the position in which the beam waist increases to $\sqrt{2}$ the size of w_0. The volume encompassed from $z = -z_R$ to $z = z_R$ is considered to be the region where most of the light is focused.

In Section 2.4 simulations of the distribution of the intensity near the focal plane of a lens (which is where the fluorophore sample is placed), are presented. Expressions are given for uniform illumination of the lens, and for illumination with a Gaussian beam.

2.4 Distribution of intensity near focal plane

As mentioned previously in Section 2.3, one of the parameters that determines the amount of fluorescence detected is the intensity provided by excitation. The intensity is

defined as

$$I(t) = \frac{P(t)}{A}, \tag{20}$$

where P is the power, and A is the area being illuminated. In order to have a significant amount of intensity, even with excitation powers as low as 0.5 nW, the size of the excitation beam was reduced by using a microscope objective to focus the light into the fluorophore sample. In the experiments, the back aperture of the objective lens was illuminated by a Gaussian profile beam, but as a first approach to obtain the spatial distribution of the intensity near the focal plane, uniform illumination was considered.

The objective is idealized as a converging thin lens of focal length f and radius a, being illuminated with a wavelength λ. Considering a Cartesian coordinate system with z along the optical axis, x' and y' are in the aperture plane of the lens, and x, y, and z define the observation point, the complex amplitude of the field is calculated through the Fresnel diffraction integral [Goodman, 1996] as

$$U(x,y,z) = \frac{e^{ikz}}{i\lambda z} \iint_S e^{-i\frac{k}{2f}(x'^2+y'^2)} e^{\frac{ik}{2z}\left[(x'-x)^2+(y'-y)^2\right]} dx'dy', \tag{21}$$

where $k = \frac{2\pi}{\lambda}$, S is the surface defined by $x'^2 + y'^2 \leq a^2$, and the amplitude incident on the lens has been assumed to be unity. Changing from Cartesian to cylindrical coordinates because of the radial symmetry of the problem,

$$x = r_2 \cos\phi \tag{22}$$

$$y = r_2 \sin\phi \tag{23}$$

$$x' = r_1 \cos\theta \tag{24}$$

$$y' = r_1 \sin\theta \tag{25}$$

The angular integration was performed using the property of the Bessel function J_o

$$J_0(\boldsymbol{\beta}) = \frac{1}{2\pi}\int_0^{2\pi} e^{-i\boldsymbol{\beta}\cos(\theta-\phi)}d\theta. \tag{26}$$

With this, the Fresnel diffraction integral can be expressed as,

$$U(z, r_2) = \frac{2\pi}{i\lambda z}\exp(ikz)\exp\left(\frac{i\pi r_2^2}{\lambda z}\right)\int_0^a \exp\left[\frac{ikr_1^2}{2}\left(\frac{1}{z}-\frac{1}{f}\right)\right] J_0\left(\frac{2\pi r_1 r_2}{\lambda z}\right) r_1 dr_1. \tag{27}$$

Then, defining the dimensionless variables u and v as

$$u = \frac{2\pi}{\lambda}\left(\frac{a}{f}\right)^2 z, \tag{28}$$

and

$$v = \frac{2\pi}{\lambda}\left(\frac{a}{f}\right) r_2, \tag{29}$$

and introducing the normalized parameter ρ as

$$\rho = \frac{r_1}{a}, \tag{30}$$

Eq. (27) can be rewritten as [Born and Wolf, 1999]

$$U(u, v) = \frac{2\pi a^2}{i\lambda f^2}\exp\left[i\left(\frac{f}{a}\right)^2 u\right]\int_0^1 J_0(v\rho)\exp\left(-\frac{1}{2}iu\rho^2\right)\rho d\rho. \tag{31}$$

The integral of Eq. (31) can be separated into real and imaginary parts as

$$2\int_0^1 J_0(v\rho)\exp\left(-\frac{1}{2}iu\rho^2\right)\rho d\rho = \mathcal{C}(u, v) - i\mathcal{S}(u, v), \tag{32}$$

where $\mathcal{C}(u, v)$ and $\mathcal{S}(u, v)$ are defined by

$$\mathcal{C}(u, v) = 2\int_0^1 J_0(v\rho)\cos\left(\frac{1}{2}u\rho^2\right)\rho d\rho, \tag{33}$$

and

$$\mathcal{S}(u, v) = 2\int_0^1 J_0(v\rho)\sin\left(\frac{1}{2}u\rho^2\right)\rho d\rho. \tag{34}$$

Equations (33) and (34) have well-known solutions [Born and Wolf, 1999] given by

$$\mathcal{C}(u,v)=\begin{cases}\frac{\cos\frac{1}{2}u}{\frac{1}{2}u}\mathcal{U}_1(u,v)+\frac{\sin\frac{1}{2}u}{\frac{1}{2}u}\mathcal{U}_2(u,v), & \text{if } |\frac{u}{v}|\leq 1\\ \frac{2}{u}\sin\frac{v^2}{2u}+\frac{\sin\frac{1}{2}u}{\frac{1}{2}u}\mathcal{V}_0(u,v)-\frac{\cos\frac{1}{2}u}{\frac{1}{2}u}\mathcal{V}_1(u,v), & \text{otherwise}\end{cases} \tag{35}$$

and

$$\mathcal{S}(u,v)=\begin{cases}\frac{\sin\frac{1}{2}u}{\frac{1}{2}u}\mathcal{U}_1(u,v)-\frac{\cos\frac{1}{2}u}{\frac{1}{2}u}\mathcal{U}_2(u,v), & \text{if } |\frac{u}{v}|\leq 1\\ \frac{2}{u}\cos\frac{v^2}{2u}-\frac{\cos\frac{1}{2}u}{\frac{1}{2}u}\mathcal{V}_0(u,v)-\frac{\sin\frac{1}{2}u}{\frac{1}{2}u}\mathcal{V}_1(u,v), & \text{otherwise},\end{cases} \tag{36}$$

where $\mathcal{U}_n$ and $\mathcal{V}_n$ (n =0, 1, or 2) are Lommel functions, defined as

$$\mathcal{U}_n(u,v)=\sum_{s=0}^{\infty}(-1)^s\left(\frac{u}{v}\right)^{n+2s}J_{n+2s}(v), \tag{37}$$

and

$$\mathcal{V}_n(u,v)=\sum_{s=0}^{\infty}(-1)^s\left(\frac{v}{u}\right)^{n+2s}J_{n+2s}(v). \tag{38}$$

With these substitutions, the distribution of intensity near the focus of the lens for the case of uniform illumination, is given by two cases (obtained as $I(u,v)=|U(u,v)|^2$). If $|\frac{u}{v}|\leq 1$ there results

$$I(u,v)=\left(\frac{2}{u}\right)^2\left[U_1^2(u,v)+U_2^2(u,v)\right]I_0, \tag{39}$$

while if $|\frac{u}{v}|>1$:

$$I(u,v)=\left(\frac{2}{u}\right)^2\left\{1+V_0^2(u,v)+V_1^2(u,v)-2V_0(u,v)\cos\left[\frac{1}{2}\left(u+\frac{v^2}{u}\right)\right]\right.$$
$$\left.-2V_1(u,v)\sin\left[\frac{1}{2}\left(u+\frac{v^2}{u}\right)\right]\right\}I_0. \tag{40}$$

In these equations, I_0 is the intensity at the geometrical focus and is defined as

$$I_0=\left(\frac{\pi a^2}{\lambda f^2}\right). \tag{41}$$

Now we consider the case in which the beam focused into the sample has a Gaussian

profile. Because of the finite size of the back aperture of the microscope objective, the beam can be truncated. Horvath and Bor (2003), found that the focusing of a truncated Gaussian beam can be treated in the same form of the previously seen solution for uniform illumination if the first variable in the Lommel functions (u) is extended to the complex domain as

$$u \to u - i2\alpha, \tag{42}$$

where α is the truncation coefficient defined as

$$\alpha = \left(\frac{a}{w}\right)^2, \tag{43}$$

where w is the Gaussian beam parameter, that corresponds to the radius to which the intensity of the Gaussian falls to $1/e^2$ of the peak. For example, uniform illumination would have $\alpha = 0$, and a high value of α would indicate a nearly untruncated Gaussian. Figure 9 illustrates a Gaussian beam profile, with the shaded area showing the case of a truncation coefficient of $\alpha = 1$.

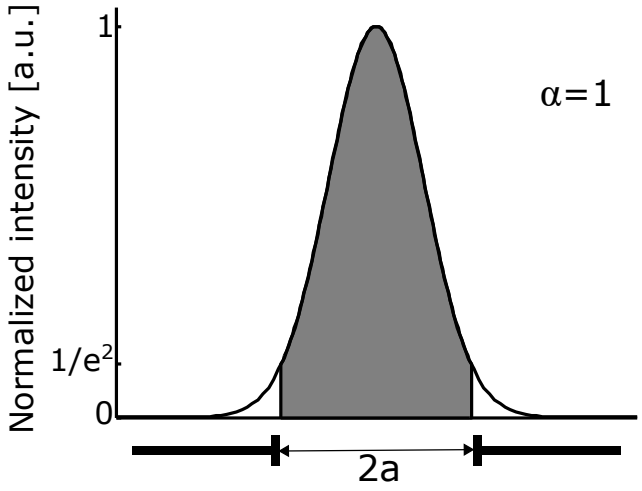

Figure 9: Truncated Gaussian beam, as illustrated by the gray area.

The solutions for the intensity distribution near the focal plane of a lens, for illumination with a Gaussian profile were plotted with MATLAB for different truncation coefficients. The parameters used where a back aperture radius $a = 3.6$ mm, wavelength $\lambda = 543$ nm, and a numerical aperture $N.A. = 0.2$ (which corresponds to a focal length of $f = 17.2$ mm). Figure 10 shows the plots obtained for this. Contours representing values of equal inten-

Table 1: First minimum of the intensity at the focal plane, for different truncation coefficients α and wavelengths λ.

α	$\lambda = 543$ nm (μm)	$\lambda = 532$ nm (μm)
0	1.63	1.60
1	1.90	1.86
2	2.33	2.29
4	4.67	4.58

sity (known as isophotes) are also shown to help distinguish the distribution. The intensity was normalized to unity at focus. The variable r_2 in Eq. (29) is expressed only as r in Fig. 10. Notice also how the position of the first minimum of intensity at the plane $z = 0$ increases with the truncation coefficient α. Table 1 compares the first minimum at the focal plane for the different truncation coefficients, and also shows cases with a shorter wavelength $\lambda = 532$ nm. It is possible to see that slightly changing the wavelength of the beam does not dramaticaly change the value of the first minimum.

From Fig. 10(b) ($\lambda = 543$ nm and $\alpha = 1$), intensity profiles at different z planes were obtained along the radial coordinate. These are presented in Fig. 11. Notice how at $z = 13.5$ μm, which is the depth of field value for the parameters used, the peak intensity has dropped to more than half of the value at focus.

The full-width at half-maximum (FWHM) dependence on position z, which was obtained by curve-fitting Gaussians to intensity profiles at different z planes, is shown in Fig. 12. It can be seen that the value of the of the FWHM increases as the z planes move further away from the focal plane.

In this work, the possibility of experimentally obtaining different truncation coefficients was provided by the design and construction of a variable beam expander. This beam expander also gave the option of adjusting the size of the beam when using microscope objectives with unalike back aperture size. In practice, only the truncation coefficient of $\alpha = 1$ was used.

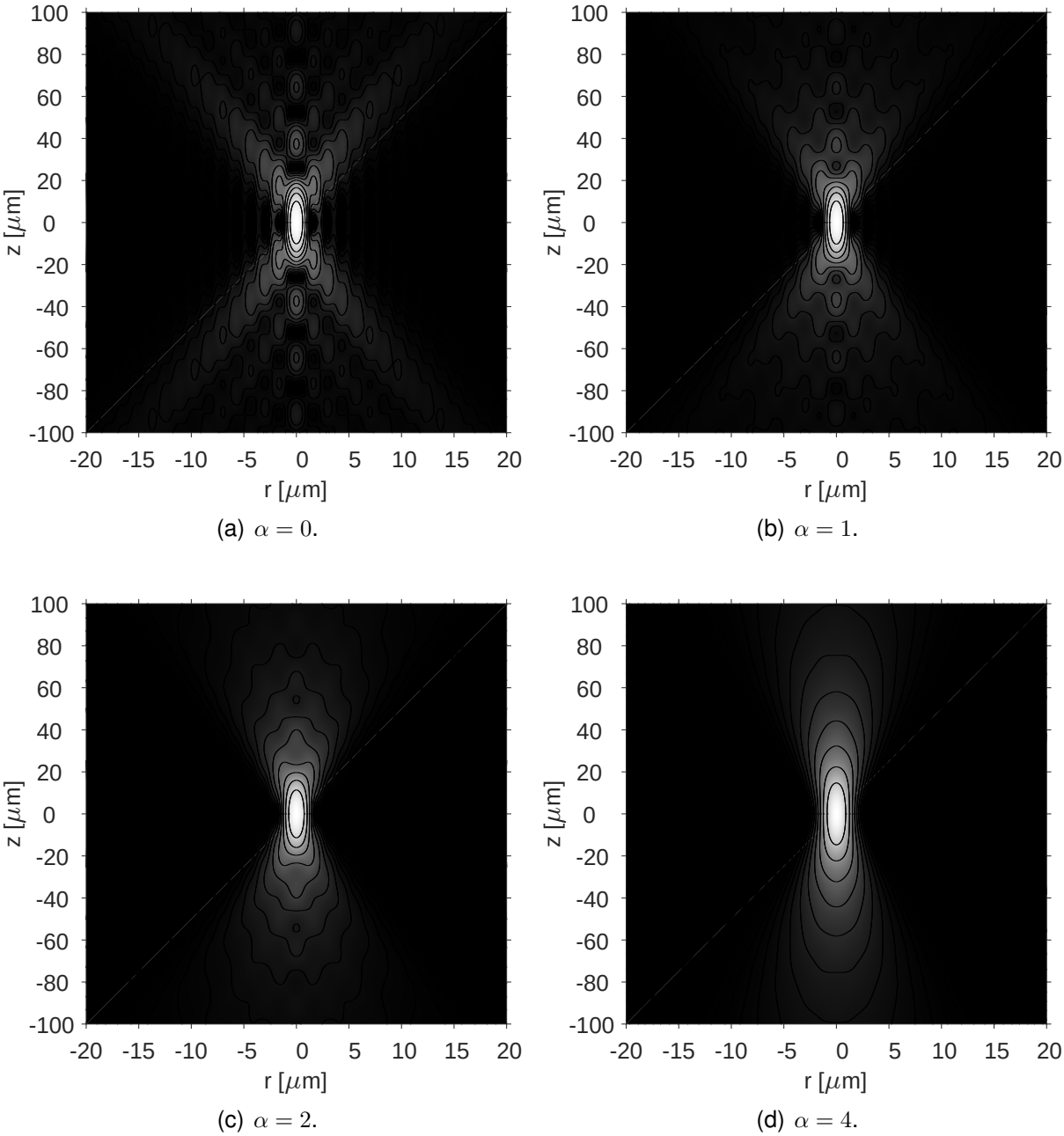

(a) $\alpha = 0$. (b) $\alpha = 1$.

(c) $\alpha = 2$. (d) $\alpha = 4$.

Figure 10: Intensity distribution near focal plane of a 0.2 N.A. lens, for a truncated Gaussian beam with truncation coefficient α as indicated.

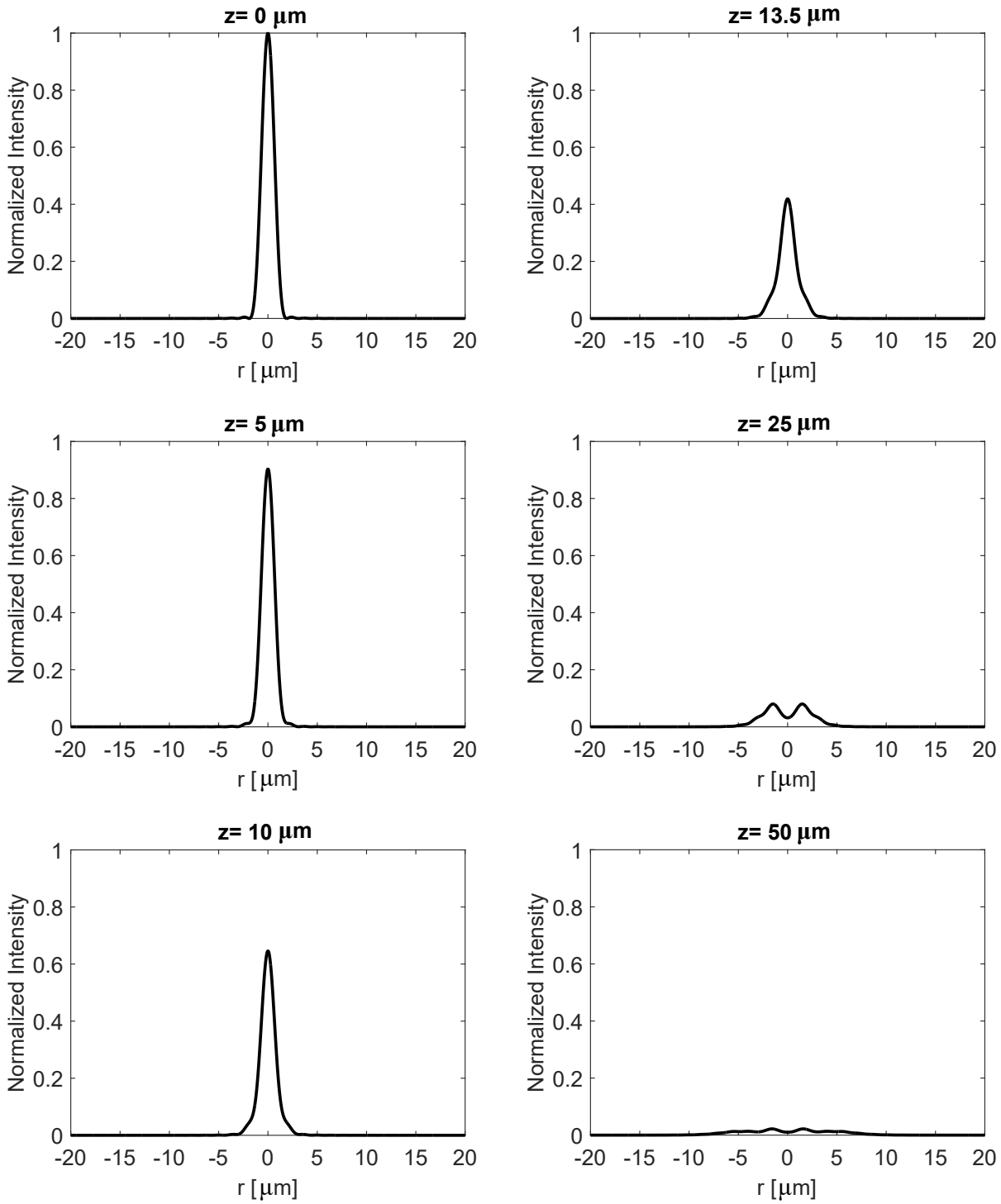

Figure 11: Radial intensity profiles for different z positions for a truncated Gaussian beam with $\lambda = 543$ nm and $\alpha = 1$.

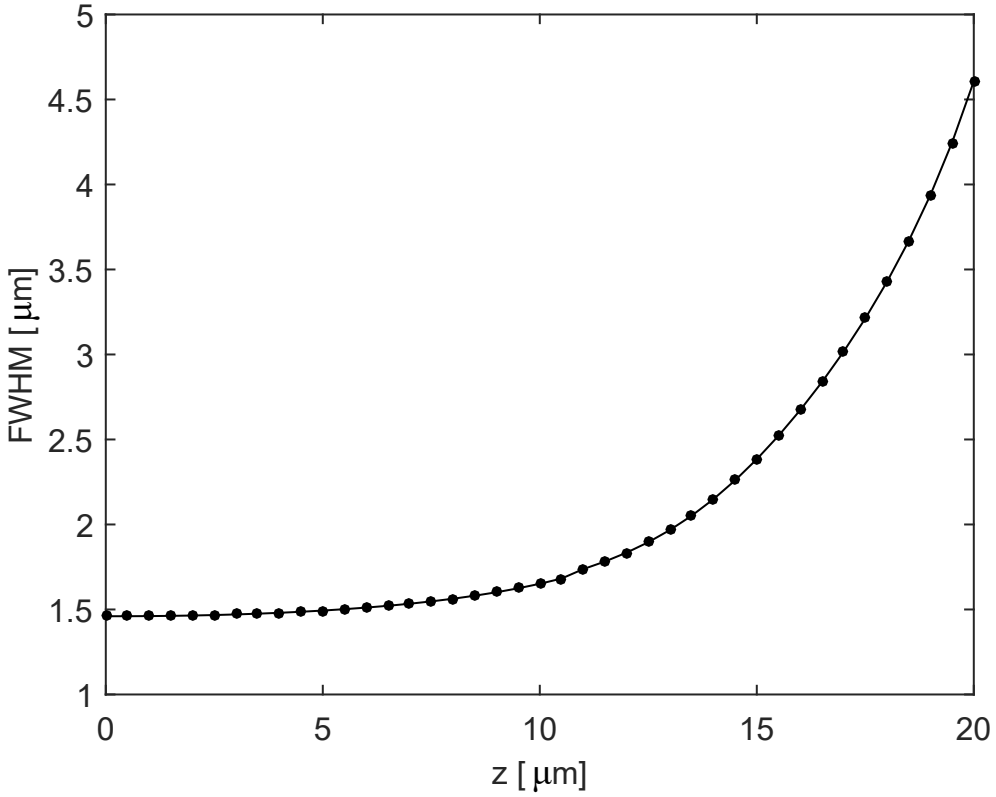

Figure 12: Dependence of FWHM on position z.

Chapter 3. Experimental System

This chapter describes the elements used to perform the experiments that were carried out for this thesis. Section 3.1 deals with the fluorophore sample, the general properties of the fluorophore, its spectral characteristics (Section 3.1.1), and the method of preparation (Section 3.1.2). Section 3.2 is about the fluorescence microscopy system and describes the components that were used to build it, their characteristics, the versatility of the system, and the options it provides. Details about the excitation source, the filters used, and the detection are presented in Subsections 3.2.1 to 3.2.3.

The experiments consisted of changing, one at a time, parameters in the sample and in the fluorescent microscopy system in order to see the influence each of them has on the fluorescence emission. The purpose of this was to find the most suitable parameters to obtain a detectable fluorescence signal by using low excitation power. The procedure for each experiment is presented alongside its result in Chapter 4.

3.1 The fluorophore sample

The fluorophore used for this project was Rhodamine B, manufactured by Sigma-Aldrich. Rhodamine B is a popular fluorescent dye that is commonly known for its use as a staining agent for cells in fluorescence microscopy [Ishii *et al.*, 1996] and as a medium in tunable dye lasers [Duarte *et al.*, 1990]. It has also been used for applications in flow cytometry, fluorescence correlation spectroscopy, and ELISA [Islam *et al.*, 2013]. It was first synthesized in 1887 by Maurice Ceresole [Sagoo, 2011], and first studied in aqueous solutions in 1924 by W.C. Holmes [Sagoo, 2011]. The physical appearance of the Rhodamine B used is that of a deep green powder, which turns pink once mixed with a solvent. The manufacturer mentions possible solvents to be water and methanol (MeOH); but others such as ethanol and ethylene glycol can also be used. The manufacturer states that for Rhodamine B dissolved in methanol, the absorption peak occurs at a wavelength of $\lambda_{ex} = 543$ nm, and the emission has a peak at $\lambda_{em} = 567$ nm. The molecular formula of Rhodamine B is $C_{29}H_{31}ClN_2O_3$, which corresponds to a molecular mass of 479.01 g /mol. The schematic of the chemical structure is shown in Fig. 13. It was obtained from the manufacturer's web page [Sigma-Aldrich, 2015], and is known as the cation form of the

fluorophore. In the space-filling model found in Fig. 13(b), each sphere represents an atom, with the radius proportional to the atomic radius and the spacing between them corresponding to the distance between their nuclei.

The solvent chosen for the experiments was methanol, because of its availability and the Rhodamine B manufacturer's recommendations. Methanol has a molecular formula given by CH_3OH and its chemical structure is shown in Fig. 14. When the Rhodamine B powder is mixed with methanol, the powder dissolves and the methanol molecules arrange themselves around each Rhodamine B molecule, creating a uniform distribution of the solute. Each solute-solvent aggregate acts as a new molecule, but there are no chemical reactions involved in the solvation. The degree of solvent influence in the fluorescence properties depends on the fluorophore, but it usually has an effect on the absorption and the emission spectrum (such as peak wavelength), and also on the quantum yield [Spring and Davidson, 2015b]. Later, in the experiments, water was tried as a solvent but, compared with the RhodamineB-MeOH sample of the same concentration, it provided poor results. According to Bindhu and Harilal (2001), the quantum yield (which can take values from 0 to 1) for Rhodamine B dissolved in water is around 0.15 lower than in methanol. Higher polarity and viscosity of the solvent increase the quantum yield for Rhodamine B [Sagoo, 2011].

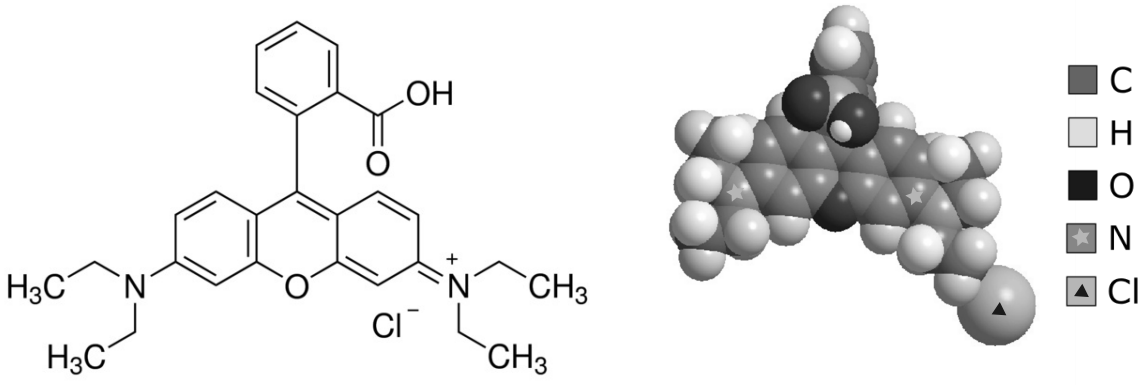

(a) Lewis/Kekule formula. (b) Space-filling model

Figure 13: Chemical structure of Rhodamine B according to the manufacturer [Sigma-Aldrich, 2015].

Another factor that influences the quantum yield is the concentration. Bindhu and

Harilal (2001) found that for methanol as the solvent, the quantum yield can range from $\eta = 0.1$ to $\eta = 0.9$ in concentrations from $C = 10^{-3}$ mol/lt to $C = 10^{-6}$ mol/lt.

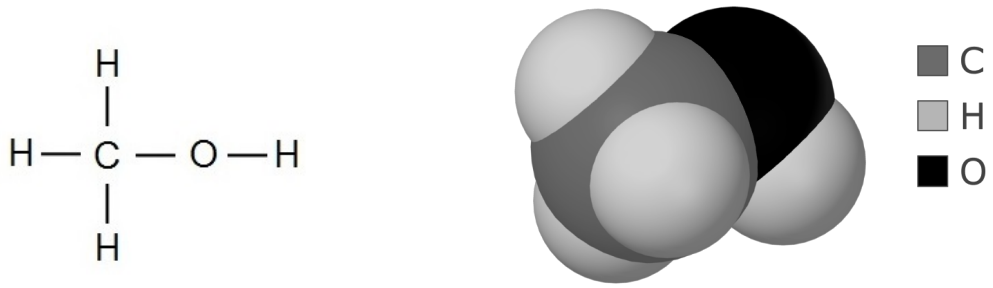

(a) Lewis/Kekule formula. (b) Space-filling model

Figure 14: Chemical structure of methanol.

3.1.1 Spectral characteristics of Rhodamine B

As can be seen in the simplified two level Jablonski diagram in Fig. 15, absorption occurs from the ground state S_0 to the first excited state S_1. For each of these states, there are vibrational energy levels (represented in the diagram by the thin horizontal lines, and labeled V_0,V_1,V_2,...,V_N). The vibrational level of S_1 to which the molecule is excited to depends on the energy the molecule had in the ground state and the energy the incident photon transferred to it when it was absorbed. The process of absorption occurs in a time frame in the order of femtoseconds. In the absence of thermal effects, the molecule usually starts at the lowest vibrational level of the ground state. The diagram shows just two possibilities of the process, both start at the same vibrational level at the ground state S_0, but the case in the left is excited with a photon of a higher energy than that of the right. The wavelength of absorption λ_a, is directly related to the energy gap ΔE between the vibrational level on the ground state and the vibrational level on the excited state of the fluorophore,

$$\Delta E = \frac{hc}{\lambda_a}, \tag{44}$$

where h is Planck's constant and c is the speed of light in vacuum.

After absorption occurs, regardless of the vibrational level that the fluorophore was excited to, the energy of the molecule decays to the lowest vibrational level of S_1 through

a process known as internal conversion. In this non-radiative process that occurs in a time frame of picoseconds, the energy is dissipated as kinetic energy. The cases shown in the diagram as squiggly arrows, go from V_N or V_1 to V_0. From there, in a time frame of nanoseconds, fluorescence occurs when the fluorophore falls to one of the vibrational levels of the ground state of S_0 with the spontaneous emission of a photon. The wavelength of the emitted photon λ_f depends again on the energy gap between V_0 of S_1 and the vibrational level of S_0. Because there are many vibrational levels in S_0 to which the molecule can fall, λ_f can have a range of values, but the emitted photon is always of a lower energy than the one absorbed.

The peak wavelength of absorption or emission may shift towards the red due to the stabilization of the ground and excited states, which manifests itself as a decrease in the energy gap between those states [Sagoo, 2011]. A blue shift is then an increase in the energy gap, and it corresponds to less stable ground and excited states. The peak position is also influenced by environmental conditions such as the solvent properties and the temperature. Because, regardless of the absorbed wavelength, the emission of fluorescence always starts from the lowest vibrational level of S_1, the emission spectrum is independent on the wavelength used for excitation.

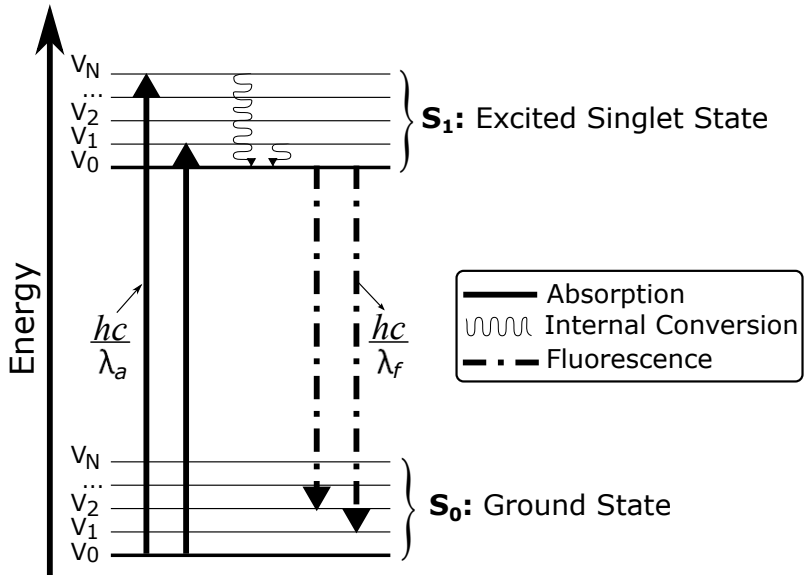

Figure 15: Simplified Jablonski diagram showing the molecular energy transitions leading to fluorescence emission. Two of the possibilities of the process are indicated with the sets of arrows.

Figure 16 shows the absorption spectrum for Rhodamine B in MeOH, for a concentra-

tion of $C = 10^{-3}$ M [Fang *et al.*, 2012]. The peak of absorption occurs at $\lambda_{ex} = 543$ nm. Figure 17 shows the measured fluorescence emission spectrum. The peak wavelength of emission was stated by the manufacturer to be at $\lambda_{em} = 567$ nm, but after measuring it with a spectrometer (Ocean Optics USB 4000), with an excitation wavelength of 543 nm and for the same solvent and concentration, it was found to be at $\lambda_{em} = 586$ nm. So, with this information, assuming the peak of absorption to be at λ=543 nm, the Stokes shift at room temperature for Rhodamine B in MeOH for a concentration of $C = 10^{-3}$ M is $\Delta\lambda = 43$ nm. The emission spectral range was found to be 96 nm, bounded by where the emission intensity fell to 10% of the peak.

There typically can be an overlap between the absorption spectrum and the emission spectrum, as illustrated by the shaded region in Fig. 18. This process can lead to the reabsorption of some of the emitted photons, which can lower the amount of fluorescence photons available for collection.

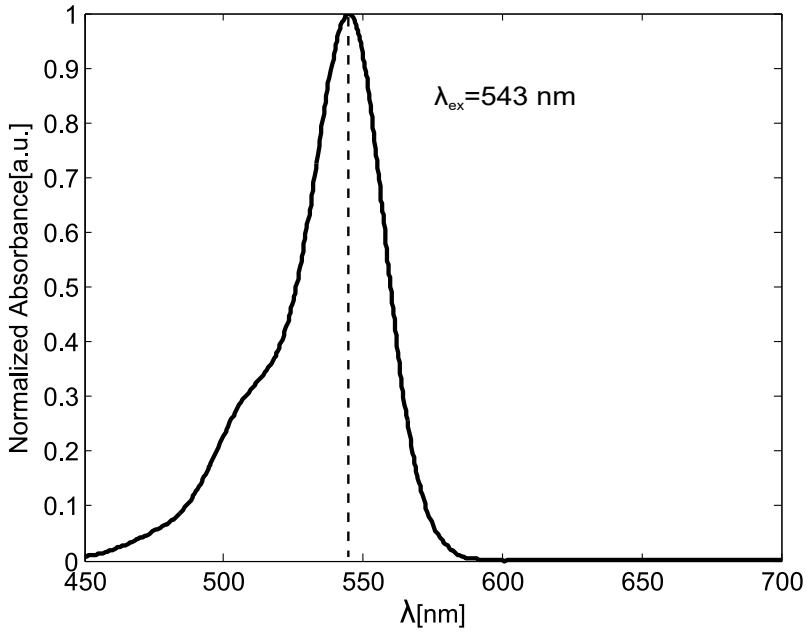

Figure 16: Absorption spectrum of Rhodamine B in methanol, for $\mathrm{C} = 10^{-3}$ M [Fang *et al.*, 2012].

3.1.2 Sample preparation

An important goal of this project is to obtain a large fluorescence signal at low excitation power, so some aspects of the sample to consider are the effects of its thickness and concentration. The samples prepared were homogeneous. They consisted of a well (50,

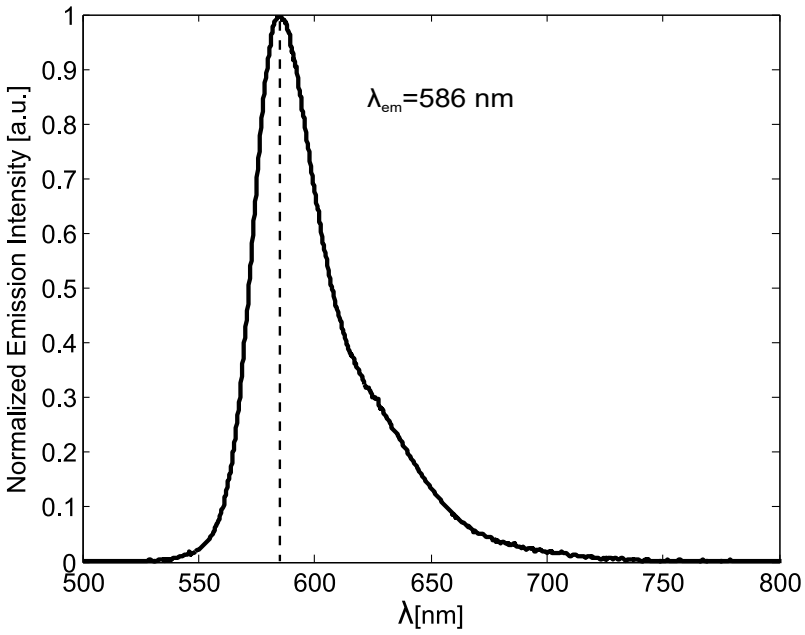

Figure 17: Measured emission spectrum of Rhodamine B in methanol, $\mathrm{C} = 10^{-3}$ M, excitation wavelength $\lambda_{\mathrm{ex}} = 543$ nm.

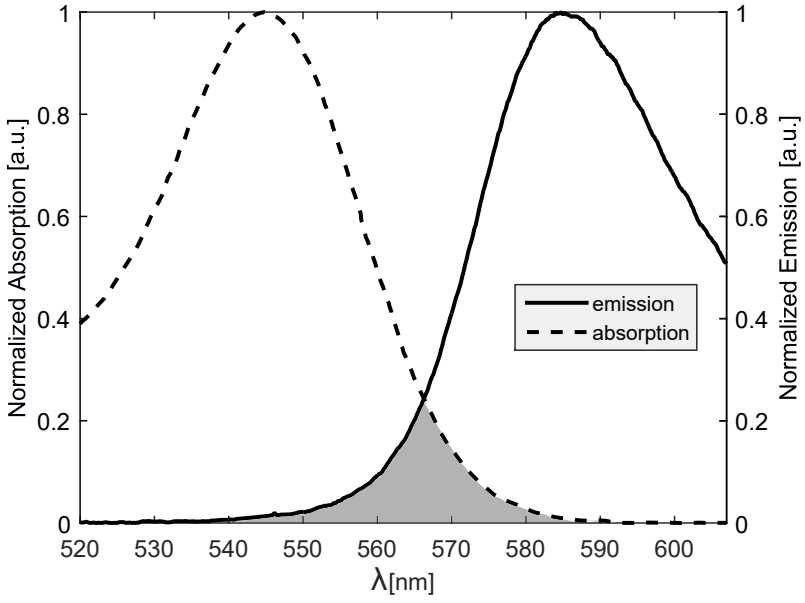

Figure 18: Plot showing the overlap of the absorption and emission spectra of Rhodamine B in methanol, $\mathrm{C} = 10^{-3}$ M.

100 or 150 μm depth) filled with the homogeneous solution of Rhodamine B in MeOH. The molar concentration C, which is expressed in mol/L or M as an abbreviation, is defined as

$$C = \frac{n_i}{V}, \tag{45}$$

where V is the total volume of the solution, and n_i is the amount of substance in the solute (calculated by dividing the number of grams of solute by the number of grams that constitute one mol of the solute).

Because the quantum yield of the fluorophore is influenced by the concentration [Bindhu and Harilal, 2001], it was interesting to see how that would influence the fluorescence measurements. Four solutions were prepared, with the concentrations being 10^{-3} M, 10^{-4} M, 10^{-5} M, and 10^{-6} M. The initial "mother" solution was obtained by measuring 0.4 mg of Rhodamine B, and adjusting the volume accordingly with Eq. (45). Because the amount of solute was small, its volume was neglected and the volume of the solvent was taken as the total volume of the solution. All other solutions were obtained through the dilution of the initial one. All containers were then kept in a dark place to avoid photobleaching before their use.

The well was prepared by layering spacers of a 50 μm thickness on top of a clean microscope slide until the desired sample thickness was obtained. It was necessary to remove with acetone any remaining glue from the spacer before placing the next. An amount of 11 μL of Rhodamine B solution per spacer was placed with a pipette at the center of the well. A coverglass (130 - 160 μm thickness) was then placed on top, and the edges were sealed using several coats of nail polish. The sample was placed on the inverted microscope stage with the coverglass facing downward, as illustrated in Fig. 19.

3.2 The fluorescence microscopy system

The experimental system was constructed using an inverted optical microscope (Nikon Eclipse TE200) as a frame. The microscope has open space at the top of its stage and at the sides, which was sufficient for the placement of some mechanical and optical elements of the excitation and collection systems (see Fig. 20). The excitation system has the purpose of providing the excitation light and guiding it to the sample at the microscope

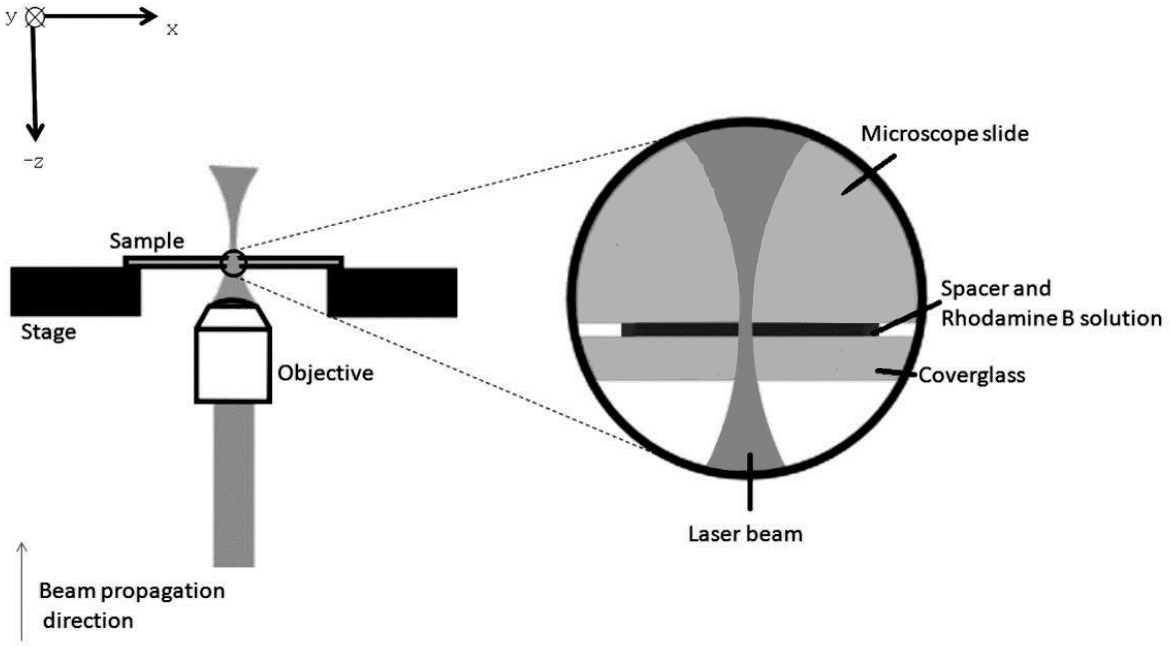

Figure 19: Structure of the fluorophore sample and its placement on the microscope stage.

stage. The collection system has the objective to gather the fluorescent light coming from the excited sample and send it to a detector so it can be measured. Both of the system configurations discussed in Section 2.1, the epifluorescent and the 4pi geometry, were constructed. The fluorescence microscopy system was built with numerous ports that give it geometric versatility and are important to perform the experiments. The locations of these ports are indicated in Fig. 20.

The *right port* of Fig. 20 was used as an input port for the excitation beam. The beam was reflected with a mirror (M_I) and the dichroic filter (DF) towards the microscope objective (Ob1), where it was focused into the sample (S). More information about the excitation is presented in Section 3.2.1.

The *top* port of Fig. 20 was used for collection in the forward direction, which corresponds to the 4pi geometry. In this geometry, the light collected with the objective Ob_2 was sent out of the *top* port with a mirror (M_T). The *back* and the *bottom left* ports were for backward collection, that is, with the epifluorescence geometry. For this configuration, fluorescence was collected with the same objective used for excitation (Ob_1), and was transmitted through the dichroic filter. The light then passed through the internal optics of

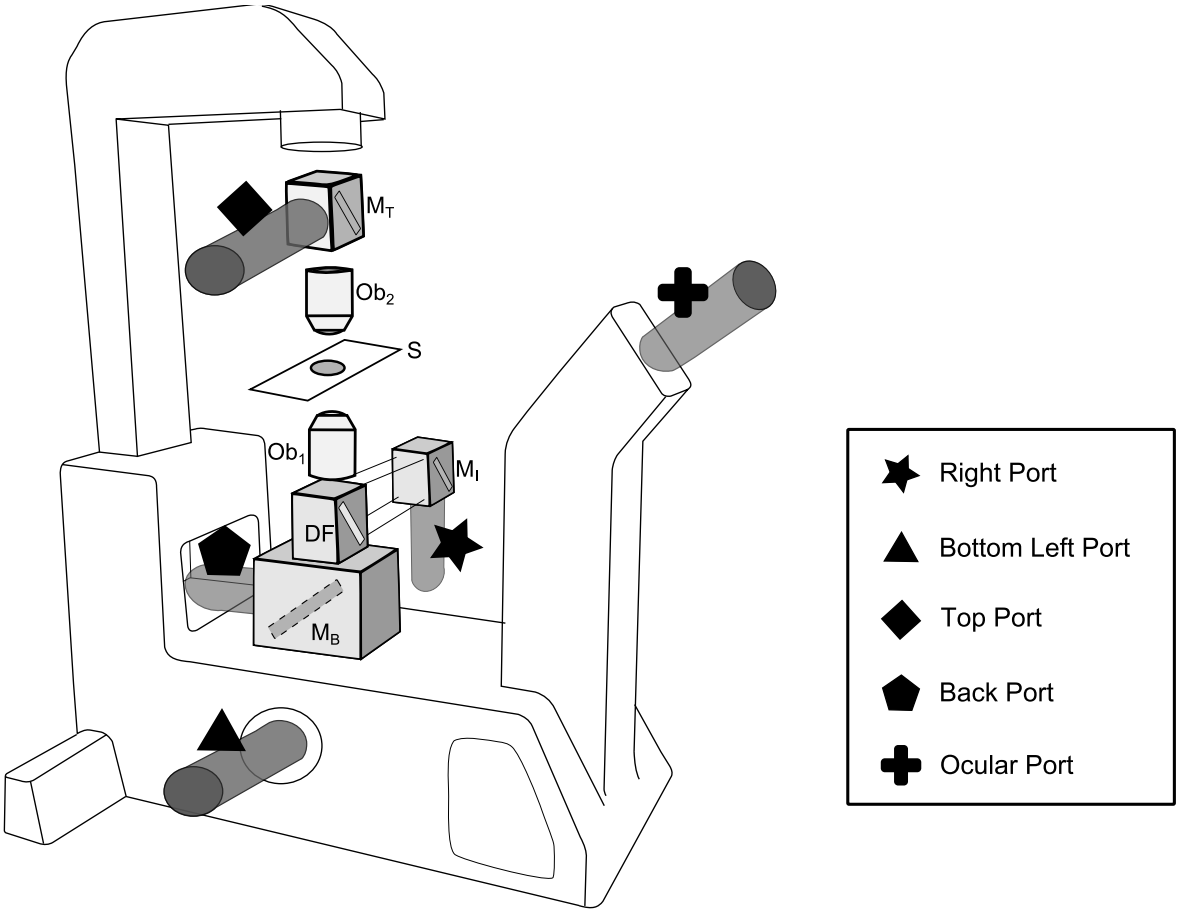

Figure 20: Inverted microscope diagram showing the input/output ports and some mechanical and optical elements of the fluorescence microscopy system. The labels for the elements are S:sample, DF:dichroic filter, M:mirror, Ob:microscope objective. The subscripts on the mirror and objective labels are referred to in the text.

the microscope and came out of the *bottom left* port. There is a space right below the dichroic filter where a mirror (M_B) could be placed to intercept the beam before it went through the internal optics, thus creating the *back* port. In all the collection options, light that remained from the excitation beam (not fluorescence) was removed by the use of an emission filter. Details about this filter, and also on the dichroic filter can be found on Section 3.2.2. More information on the collection system and the detection is provided in Section 3.2.3.

To optimize the excitation intensity arriving at the Rhodamine B sample, it is important to know the position of the beam waist. In order to investigate what focusing position yielded the highest fluorescence signal, the objective labeled as Ob_1 in Fig. 20 could be moved with the focusing knob of the inverted microscope, with a resolution of 1 μm. Likewise, to adjust the position of the collection volume in the 4pi geometry, the objective labeled Ob_2 was mounted with a dial gauge having a resolution of 25 μm.

To position the sample on the microscope stage, and also to align the excitation beams, spatial information was obtained with the use of a CCD camera (Pulnix, TMC-7ex). The CCD camera was located at the *ocular* port of the microscope, with the ocular removed, so as to capture the intermediate image of the sample (S) produced by the microscope objective (Ob_1) of Fig. 20. The camera was connected to a monitor placed next to the microscope.

3.2.1 The excitation

Three different sources could be selected for excitation in the fluorescence microscopy system. Figure 21 shows the schematic of the options. As illustrated already in Fig. 16, the Rhodamine B solution ($C = 10^{-3}$ M) has a peak of absorption at $\lambda = 543$ nm. In order to maximize the fluorescence signal, a green He-Ne laser matching that wavelength was used as an excitation source (labeled as L_{543} in Fig. 21). Its output power was measured to be 1.1 mW. The beam had a TEM_{00} Gaussian profile, with a diameter of 0.83 mm and a divergence of 0.84 mrad. The availability of a cw Nd:YAG laser with $\lambda = 532$ nm (L_{532}) allowed for the study of what would happen to the fluorescence signal if a wavelength off of the absorption peak (for $\lambda = 532$ nm it is 31% less than for $\lambda = 543$ nm) was used for

excitation. Saturation of the fluorescence signal can occur by illuminating the Rhodamine B sample with a high intensity, so, with the purpose of finding the saturation intensity, an 800 ps pulsed Nd:YAG laser (L_{532P}) with a repetition frequency of 20 kHz and $\lambda = 532$ nm, was also used (see Subsection 2.3.6, in Chapter 2). Any of the three excitation sources described earlier could be chosen to be sent into the *right* port of the microscope with the use of flip mirrors (FM).

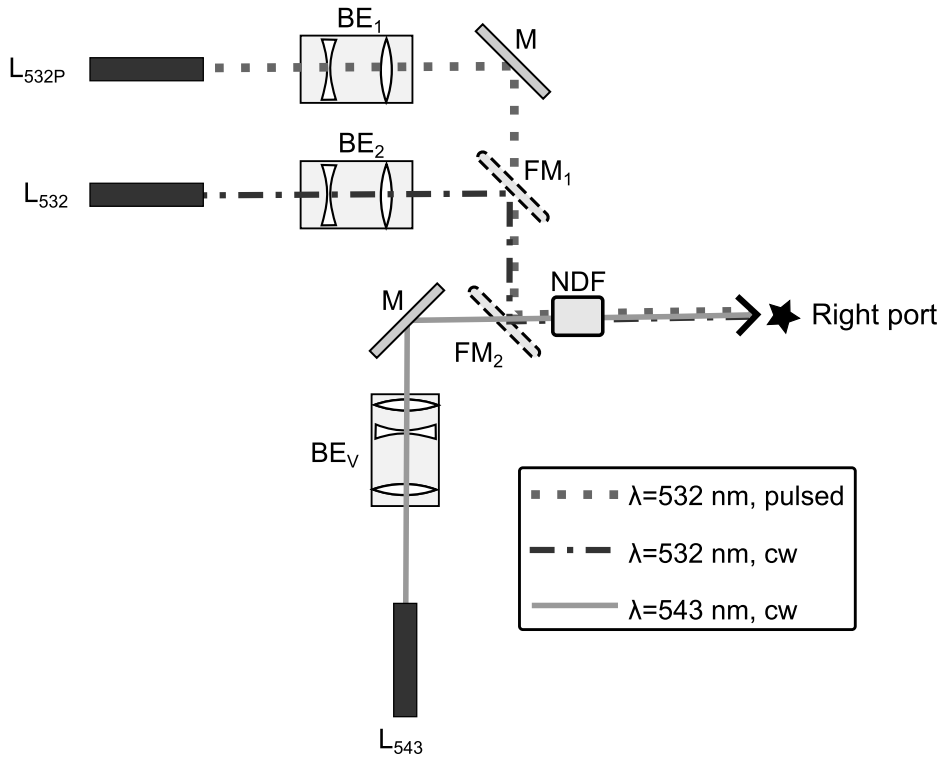

Figure 21: Schematic showing the options for the excitation source. The label meanings are L: excitation laser, BE: beam expander, M: mirror, FM: flip mirror, and NDF: neutral density filters

The microscope objective chosen to focus the excitation beam had a magnification of 10x, a N.A. of 0.2, and a back aperture diameter of 7.3 mm. Underfilling the objective's back aperture leads to an increased focused spot size. Overfilling it generates power losses. In order to minimize the spot size and the power losses, the beam diameters were changed with beam expanders (BE) to achieve a truncation coefficient of $\alpha = 1$ as shown in Chapter 2, Fig. 9. Because different microscope objectives have different back aperture diameters, a variable beam expander (BE_V) was designed and constructed for the L_{543} laser (see Fig. 22). By adjusting the separation between the lenses, l_1 and l_2, the beam could be collimated and the initial diameter of the beam d_i could be increased to d_f. In

this thesis, only work with the 10x microscope objective is presented, so the lens positions were fixed to yield $d_f = 7.3$ mm.

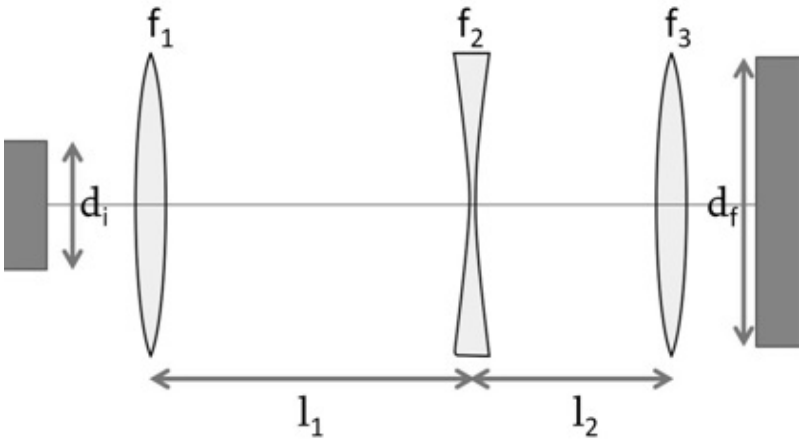

Figure 22: Schematic of the variable beam expander. The focal length of the lenses are: $\mathbf{f_1 = 100}$ mm, $\mathbf{f_2 = -50}$ mm, $\mathbf{f_3 = 120}$ mm.

The excitation power reaching the microscope stage could be changed with neutral density filters (NDF). The optical densities ranged from 0.13 to 3.97, making possible the reduction of the excitation power to 0.05 nW.

3.2.2 The filters

Filters play an important role in the fluorescence microscopy system because they are needed to separate the emitted fluorescence from the excitation light. From the emission spectrum shown previously in Fig. 17, it can be seen that a filter that will transmit the emitted photons in the range of 561 nm to 657 nm, while blocking the shorter excitation wavelengths, is needed for the collection system.

Furthermore, in the epifluorescence configuration, the key element that allows excitation and collection with the same microscope objective is a dichroic filter (labeled DF in Fig. 20). The dichroic filter was used in the excitation system to reflect the excitation source towards the microscope objective (Ob_1). For the wavelengths used for excitation, the reflectivities are R($\lambda = 543$ nm)=95.2% and R($\lambda = 532$ nm)=96.4%. In the backward collection system, it allows a more than 10% transmission of the wavelengths between 548 and 596 nm, with the transmission at the peak emission wavelength being

T($\lambda = 586$ nm)=25.4$\%$. The measured transmission spectrum of the dichroic filter used is shown in Fig. 23. It can be seen that although this dichroic filter is not ideal, it does effectively reflect the excitation wavelengths, and it does partially transmit longer wavelengths at which fluorescence occurs (including the emission peak). If fluorescence photons can be detected with this dichroic filter, a higher signal can certainly be obtained by using a more efficient one.

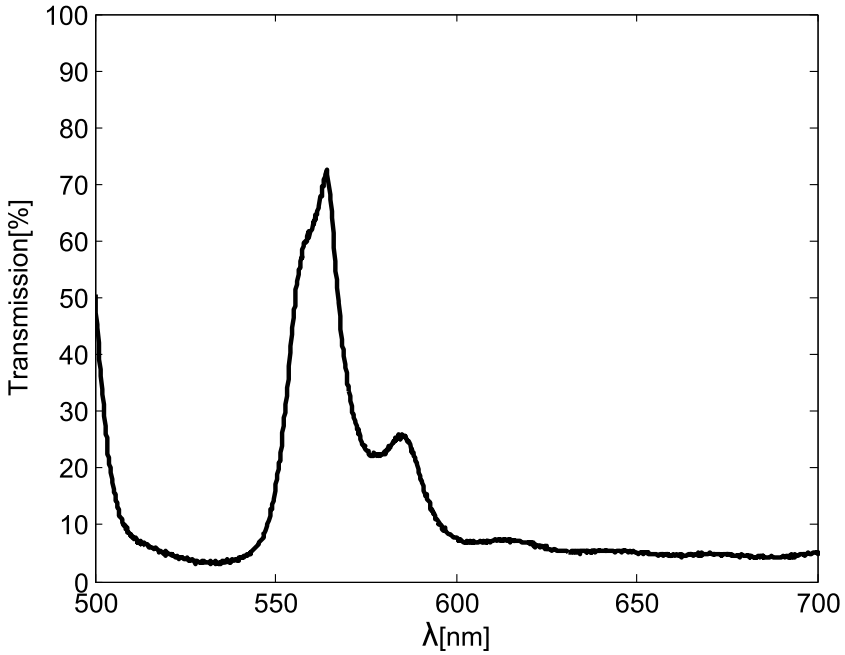

Figure 23: Transmission spectrum of the dichroic filter.

The transmission spectra of the emission filters can be seen in Fig. 24. The emission filter (labeled as EF_B or EF_T) was used in the collection so that light from the excitation source could not reach the detector. For the case of backward collection, because the dichroic filter has a low transmission of the excitation wavelengths, it was enough to use a bandpass filter (TRITC). For forward collection, in which there is no dichroic filter in the optical path, the TRITC filter was used in conjunction with a multibandpass filter.

The total effect of the filters in the shape of the collected light spectrum is presented in Fig. 25. In Fig. 25(a), the detected light in the backward collection is shown (passing through dichroic and EF_B). Figure 25(b) shows it for forward collection (passing through EF_T). Each of the spectra is normalized to unity in order to better appreciate the window of collection for the two geometries. It is noted that the fluorescence emission peak does

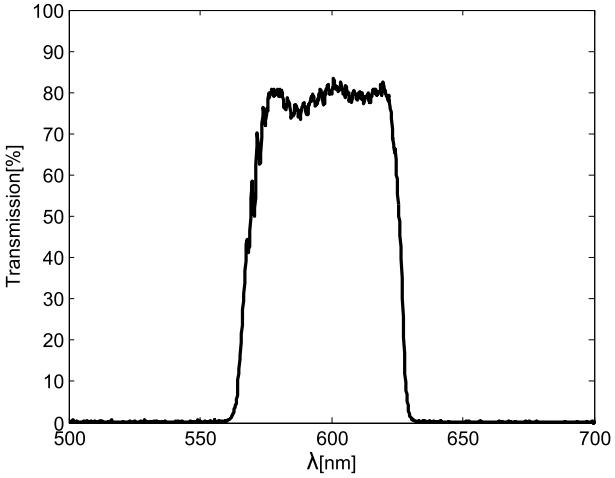

(a) Bandpass TRICT filter (EF_B).

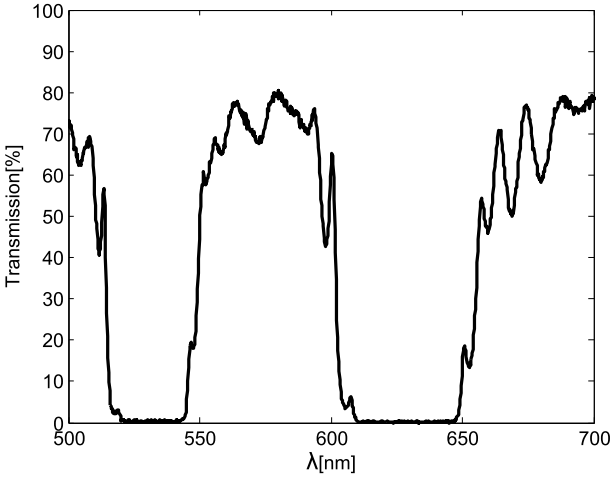

(b) Multibandpass optical rejection filter.

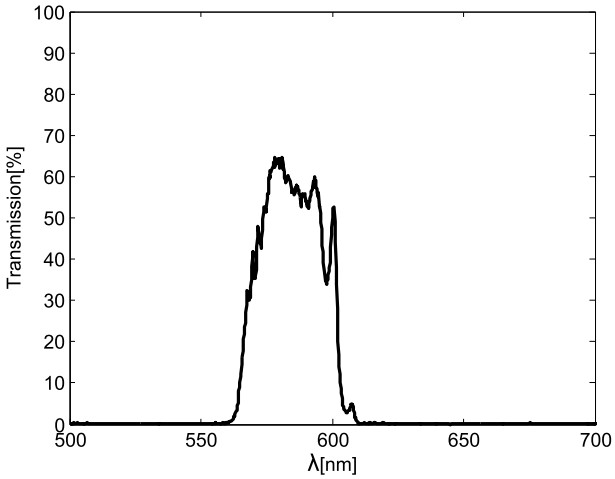

(c) Product of TRITC and optical rejection filters (EF_T).

Figure 24: Transmission spectra of the emission filters.

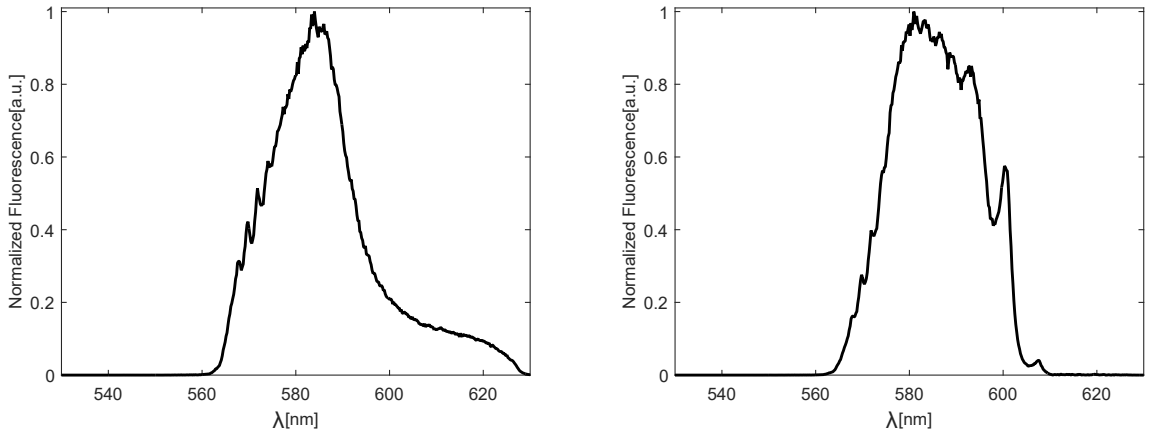

(a) Backward collection (b) Forward collection

Figure 25: Normalized fluorescence emission spectrum after passing through the filters used for collection. It is shown for two different collection geometries.

fall within the wavelength range transmitted by the filters, and that light coming from the excitation source is completely blocked.

It was mentioned previously in Section 3.1.1, that the overlap between the absorption and emission spectrum can lead to reabsorption. However, because the lasers used for excitation are not of wavelengths in the region of overlap, and also because the emission in the overlap wavelengths is poor, there is only a small probability of reabsorption occurring, and the probability of reemission is even less.

3.2.3 The detection

When non-polarized light is used as excitation, the emission of fluorescence has no preferential direction and it is emitted in an isotropic distribution. In contrast, when a fluorophore sample is excited with linearly polarized light, the molecules whose transition moments are oriented in a direction close to that of the electric vector are the ones that are preferentially excited, and thus, the emitted fluorescence also has a preferential direction [Valeur, 2001]. Nevertheless, if the excited molecules can rotate freely before emission, then the emission loses some of its anisotropy and can even become a nearly isotropic distribution. Then, if fluorescence is emitted in all directions, the amount of emitted light reaching the detector is determined by the optics of the collection system. Three collection paths where constructed and then compared to determine the most efficient one.

Figure 26 shows a schematic of the collection system options. The ports illustrated in this figure represent the same output ports of Fig. 20, already discussed in Section 3.2. For collection in the *forward* direction, the thickness of the sample was an important parameter because the emitted fluorescence has to be transmitted through part of the sample before it can be captured with a microscope objective (labeled Ob_2 in Fig. 26). The light gathered by the objective was reflected from the *top* port with a mirror (M_T), where the emission filter (EF_T) blocked residual light from the excitation source. A positive lens (labeled PL in Fig. 26) could then be used to focus the remaining light into the detector (D). For collection in the epifluorescence geometry there were two options. In both cases fluorescence was gathered with the objective used for excitation (Ob_1), and then it was partially transmitted by the dichroic filter (DF). For the path labeled *backward through microscope base*, the light passed on through the internal optics of the microscope and emerged from the *bottom left* port. The emission filter (EF_B) was placed in the path before the detector. In the path labeled only as *backward*, a mirror (M_B) was placed to reflect the collected light to the *back* port, so that it wouldn't pass through the internal components of the microscope. The detector was then placed as in the *forward* path, but using EF_B as the emission filter. The reason for the two backward collection options was to see if significant losses in transmission due to the internal components of the microscope occurred, in which case a higher signal would be obtained by using the *back* port.

In this project, the detection was carried out in two forms. One form was through the recording of images of the fluorescence and the excitation beams with a CMOS camera (Thorlabs, DCC1545M). The other form was measuring a signal proportional to the collected light, resulting from the use of a photomultiplier (Hamamatsu 1P21). The photomultiplier (PMT) was more sensitive than the camera.

For the recording of images, the *bottom left* port was used. The field of view (with the 0.2 N.A., 10x objective) was calibrated with a reticle that had 0.02 mm as the smallest scale. It was found that the 1280×1024 CMOS pixels corresponded to a field of view of 533×426 μm.

The PMT was supplied with 800 V from a high voltage power supply (Pacific Instruments 204). The PMT signal was sent to a digital multimeter (Keithley 187), which was

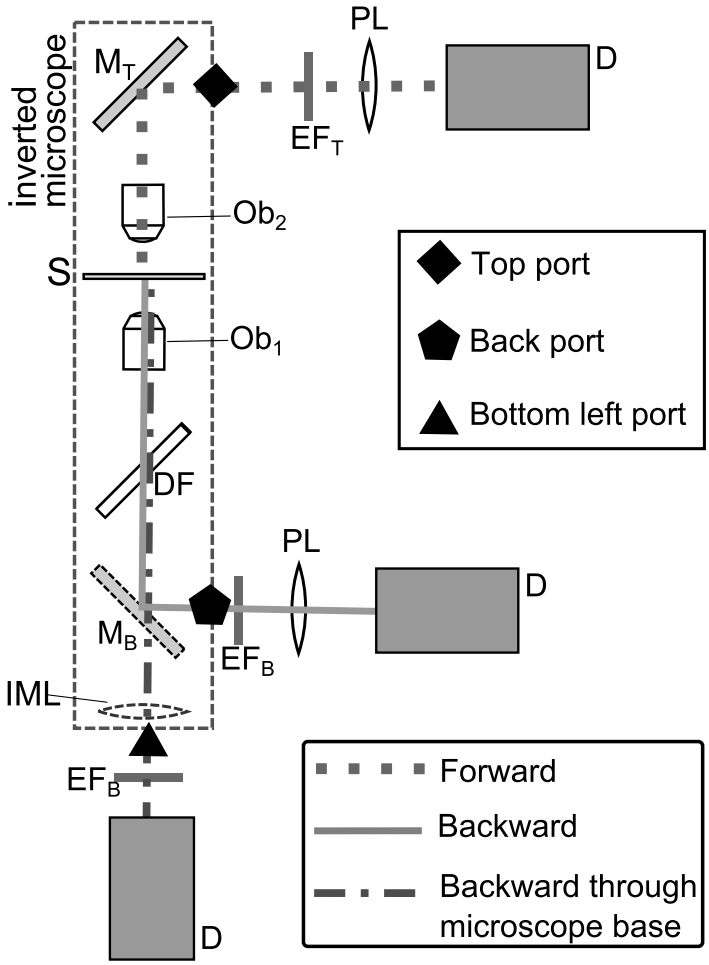

Figure 26: Schematic of the different paths of the collection system. S: Sample, Obj: Microscope objective, DF: Dichroic Filter, M: Mirror, EF: Emission Filter, PL: Positive lens, IML: Internal microscope lens, D: Detector

connected to a computer (Linux Mint 15) via a GPIB-USB-HS interface (National Instruments). Programs in C were used to monitor and record the data provided by the PMT. The focal length of the lens (labeled PL in Fig. 26) used to concentrate the collected light into the photocathode of the sensor for collection through *top* or *back* ports was $f_l = 100$ mm. It should be recalled that no additional lens was used for collection with the *bottom left* port due to the focusing already provided by the internal components of the microscope (labeled IML in Fig. 26).

Chapter 4. Results and Discussions

In this chapter, the experimental results are presented and analyzed. It is divided in subsections, each dealing with one of the studied parameters. In Subsection 4.1, images of the excitation beam and the fluorescence spot are shown and compared. Subsection 4.2 and Subsection 4.3 deal, respectively, with the roles that fluorophore concentration and sample thickness play in the fluorescence emission. The importance of the focusing position of the excitation beam in the sample is discussed in Subsection 4.4. Comparisons of excitation with sources of different wavelength are presented in Subsection 4.5. In Subsection 4.6, the results of exciting the fluorophore sample with pulsed and continuous sources of the same wavelength are shown, and information of saturation intensity and absorption cross-section is extracted from the pulsed excitation data. In Subsection 4.7, a comparison of the fluorescence obtained by using the different collection geometries constructed is done. The peak position dependence on fluorophore concentration and on excitation source is explored in Section 4.8. Finally, low power fluorescence measurements are presented in Section 4.9.

4.1 2D images of the excitation beam and the emitted fluorescence

A PMT can be of use for detecting low levels of light but, unlike a camera, it does not directly provide spatial information. To obtain images of the excitation beam and the produced fluorescence, the camera was aligned at the *bottom left* port of the fluorescence microscopy system, as discussed previously in Fig. 26 of Chapter 3, Section 3.2.3. The He-Ne laser with $\lambda = 543$ nm was chosen as the excitation source, and the power arriving at the microscope stage was adjusted to 11 μW with the neutral density filters. For the excitation beam image, the emission filter was removed from the collection system, and a non-fluorescent sample was employed. In the case of the fluorescence image, the emission filter was placed in the system, and a Rhodamine B sample of 100 μm thickness and a concentration of $C = 10^{-3}$ M was used.

The acquired images for excitation and fluorescence can be seen, respectively, in Figs. 27(a) and 27(c). It should be noted that the excitation beam looks quite defined, while the fluorescence appears to be more of a cloud. The cross-section profile of the

excitation was obtained, and is seen as compared with a Gaussian function in Fig. 27(b). The lower intensity peak to the right of the maximum is probably due to reflections of the fluorescence microscopy system's optical components. With the Gaussian fit, the full-width at half-maximum (FWHM) was found to be 3.8 μm. For the fluorescence, the camera settings were adjusted to produce a clearer image, which also increased the background noise, as can be seen surrounding the main peak of the cross-section profile in Fig. 27(d). By fitting a Gaussian function to the fluorescence profile, the FWHM was found to be 38.0 μm, which is 10 times larger than the FWHM obtained for the excitation.

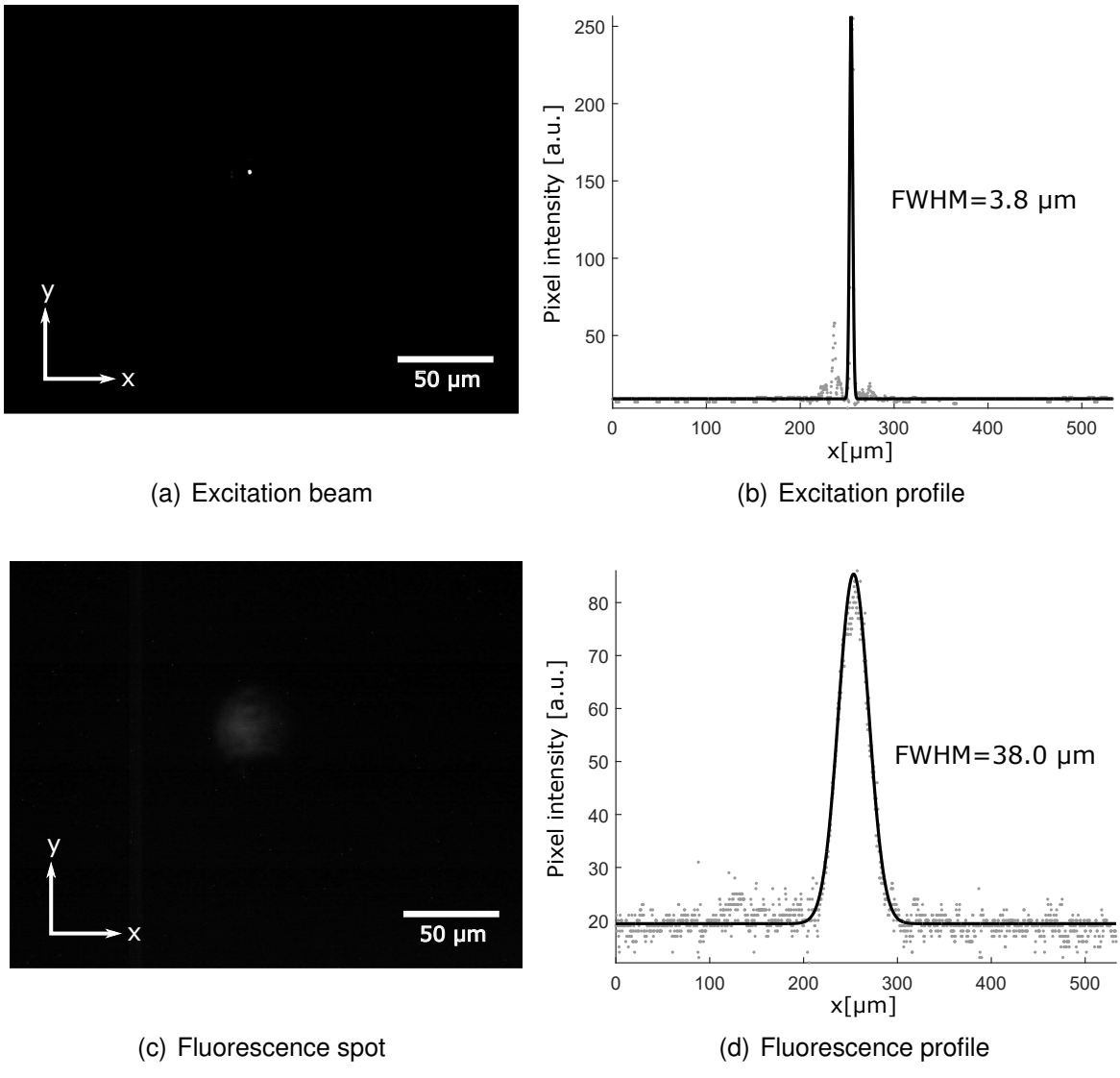

(a) Excitation beam

(b) Excitation profile

(c) Fluorescence spot

(d) Fluorescence profile

Figure 27: Images of the excitation beam and fluorescence spot.

To determine how the size of the collected fluorescence spot was influenced by the

focusing position, starting from the place between the Rhodamine B solution and the microscope slide (See Fig. 19, Chapter 3), images were taken going downwards every 5 μm, until it was very difficult to distinguish the fluorescence spot from the background. The sample used for this was of concentration $C = 10^{-3}$ M and thickness of 50 μm. For each of the images taken, a Gaussian was curve-fitted and the FWHM was obtained. The results can be seen in Fig. 28.

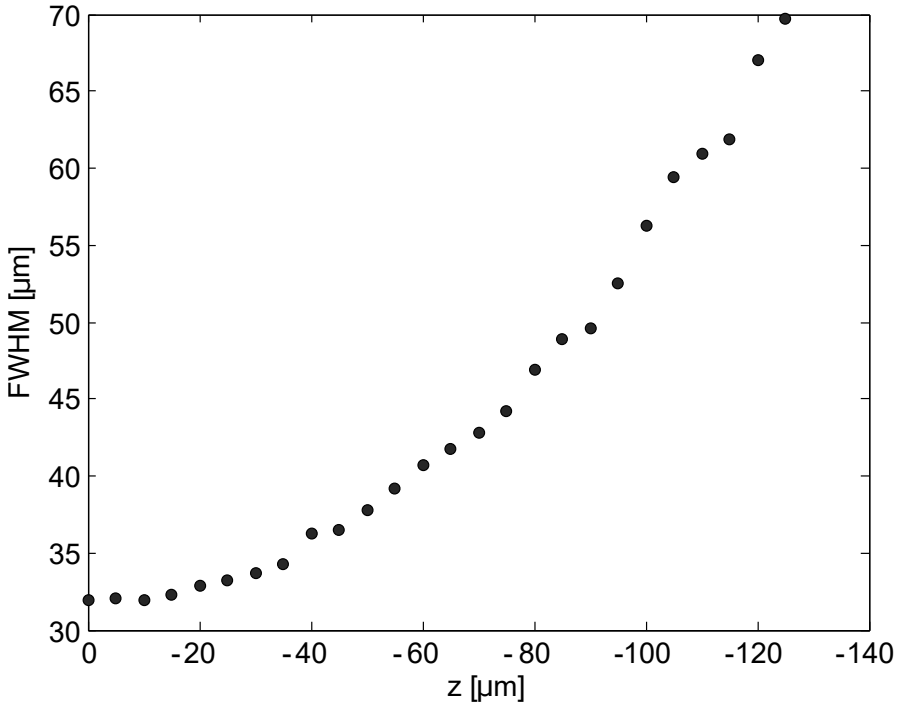

Figure 28: Full-width at half-maximum (FWHM) of the recorded fluorescence spot, in relation to the focusing position z.

It can be seen that for this 50 μm sample, the FWHM at z=0 was smaller than what was obtained with the 100 μm thickness.

4.2 Concentration of the fluorophore sample

To see the influence that the concentration had on the fluorescence emission, samples having the same 50 μm thickness but different concentrations were studied. The concentrations of the samples prepared, as mentioned in Section 3.1.2, were C$= 10^{-3}$ M, C$= 10^{-4}$ M, C$= 10^{-5}$ M, and C$= 10^{-6}$ M. The excitation source used was the $\lambda = 543$ nm He-Ne laser. The PMT was placed at the *top* output port, in the forward collection configuration (See Fig. 26 of Section 3.2.3). For each sample, the fluorescence signal was recorded

changing the excitation power arriving at the stage. For each data point, the sample was illuminated for less than 4 seconds to try to prevent photo-damage. Figure 29 shows the results obtained for this experiment. As can be seen from the straight lines fitted to the results of Fig. 29, all concentrations have a linear relationship with the excitation power, as is to be expected for absorption that occurs as a one-photon process (linear absorption) in the absence of photobleaching or saturation.

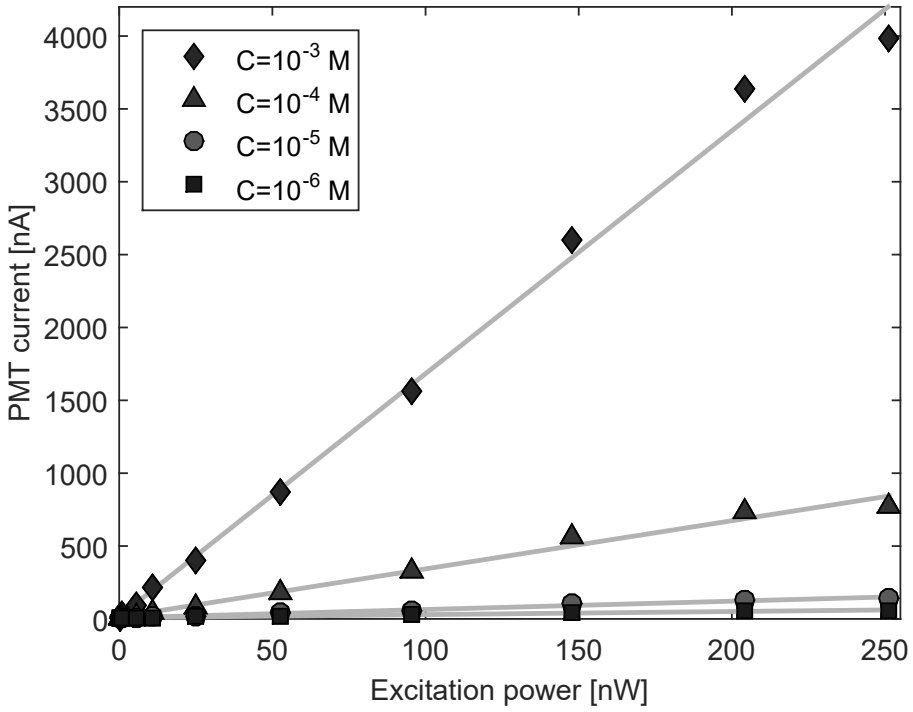

Figure 29: Fluorescence signal (PMT current) dependence on the excitation power for samples with different concentrations.

Something else that can be seen from Fig. 29, is that the higher the concentration of the fluorophore sample, the higher the fluorescence signal. As had been seen from Eq. (15) (Section 2.3), for a sample in which there is no photobleaching or saturation, the collected fluorescence is proportional to the concentration of the fluorophore solution.

The fluorescence signal was measured for the four samples of different concentration, with a fixed excitation power of 50 nW. A comparison between them was made taking the highest fluorescence signal as 100%. Figure 30 shows the results obtained. There is a difference in concentration of 10^{-1} between each consecutive column in Fig. 30, however this relationship in the fluorescence signal percentage does not apply. It is possible that the

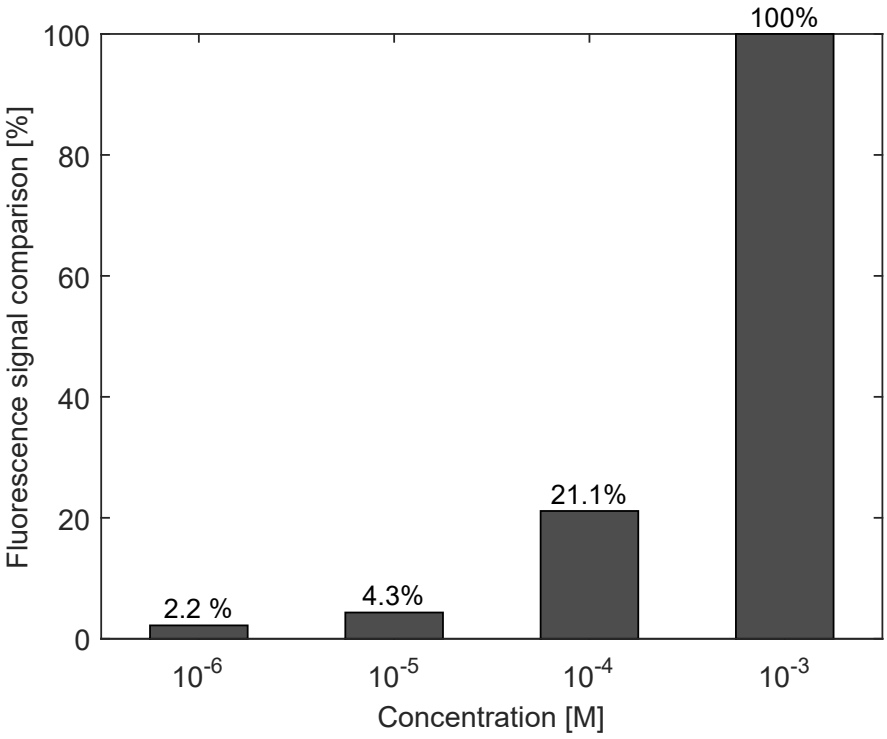

Figure 30: Comparison of the fluorescence signal for samples having four different concentrations.

quantum yield dependence on the concentration [Bindhu and Harilal, 2001] is responsible for the discrepancy.

Another effect that was studied regarding the concentration of the fluorophore sample was the position of the fluorescence emission peak. The results for this can be found in Section 4.8.

4.3 Sample thickness

From the Beer-Lambert law, it is known that in transmission, thick samples can be a problem due to the attenuation of the excitation beam. However, when collecting in reflection, the influence that the thickness of the sample has on the collected fluorescence is not clear. To investigate this, two samples, one with 50 μm thickness and one with 100 μm thickness, were prepared. Both had a concentration of C=10^{-3} M. The PMT was placed at the *bottom left* port and the fluorescence signal for each sample was recorded for a series of excitation powers. The wavelength of excitation was λ=543 nm. Figure 31 shows the results obtained from this experiment. The thicker sample yielded a higher

fluorescence signal, regardless of the excitation power.

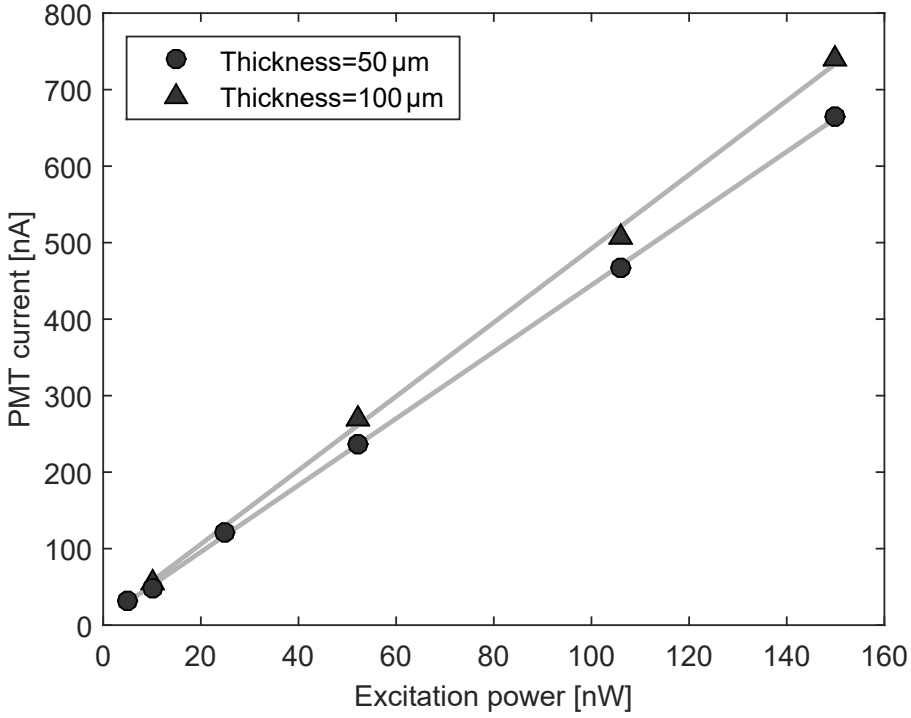

Figure 31: Fluorescence signal (PMT current) with respect to excitation power, for samples of different thickness.

Afterwards, samples with the same C=10^{-3} M concentration and three different thickness were prepared. In this case, the excitation power incident on the sample was fixed to 50 nW and the *back* port was used. The excitation wavelength used was again λ=543 nm. The fluorescence signals obtained from the excitation of samples of different thickness where compared, taking the highest value to be 100%. This highest value corresponded to the thickest sample. The results are shown if Fig. 32. The signal obtained with the 100 μm sample was 90% of what was obtained with 150 μm thickness. The fluorescence signal obtained with the thinnest sample (50 μm), was only 16% less than that obtained with the thickest one (150 μm). It can be seen then, that for collection with an epifluorescent geometry, the thickness of the sample does not have a dramatic influence on the collected fluorescence signal, because tripling the thickness only increases the fluorescence signal by 16%. Due to this, and also to the fact that the thicker the sample, the more difficult it was to prepare correctly, in the later experiments mostly samples of 50 μm thickness were used.

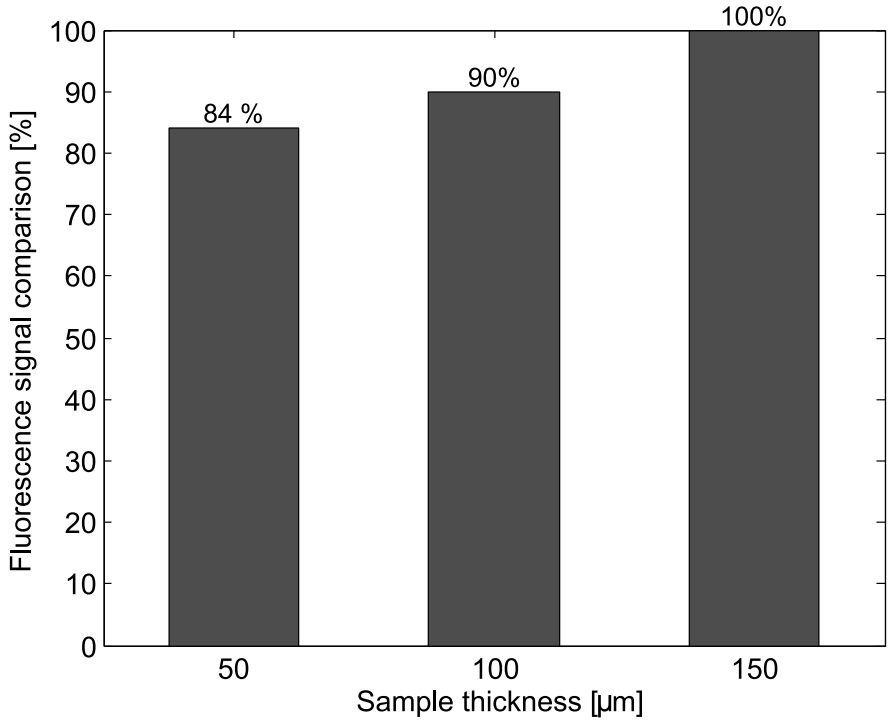

Figure 32: Fluorescence signal (PMT current) comparison for samples of different thickness.

4.4 Focusing position of the microscope objective

Another matter of interest was to find in which z axis position should the microscope objective be placed to achieve the highest fluorescence signal. To do this, a scan in z was performed using the microscope's focusing knob. The PMT was placed at the bottom left port, in the backward collection configuration. The focusing knob was calibrated so as to have the interface between the Rhodamine B solution and the microscope slide of the sample be the zero. Scanning over a range of ± 200 μm, the fluorescence signal was recorded every 20 μm. Figure 33 shows the results obtained for this experiment. It can be seen that, even when focusing 200 μm above the part of the sample containing the fluorophore solution, there is still a significant signal recorded. The fluorescence signal increases as the beam waist comes near the Rhodamine B solution when coming from above, but it remains almost constant after that. It appears to start decreasing again around 100 μm below the Rhodamine B solution, but more slowly. Due to the mechanical limitations of the microscope, it was not possible to have reliable data below z=-200 μm. The depth of field for the microscope objective used was 13.5 μm.

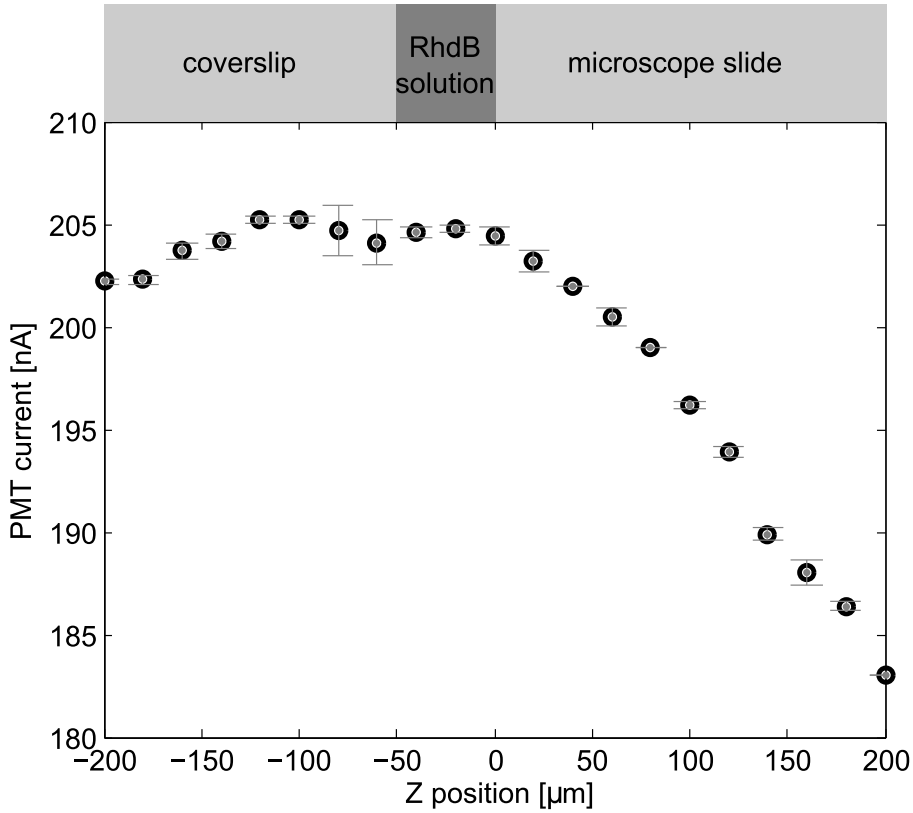

Figure 33: Fluorescence signal (PMT current) in relation to the focusing position in the sample. The sample used had a 50 μm thickness and a concentration C=10^{-3} M.

4.5 Wavelength of excitation

The absorption peak of a fluorophore can be influenced by the properties of the solvent. It was seen in Section 3.1.1, that the absorption peak wavelength for Rhodamine B in MeOH occurs at $\lambda = 543$ nm. A He-Ne laser of that exact wavelength was available for this project, and it is natural to believe that this source would be the best-suited for the excitation of the fluorophore. Nonetheless, there was also an interest to see what would happen if a wavelength slightly off the peak of absorption was used. Due to the construction of the excitation system (See Fig. 21 in Section 3.2.1), it was possible to easily change between the $\lambda = 543$ nm and the $\lambda = 532$ nm cw sources.

For the experiment comparing the two excitation wavelengths, the PMT was positioned at the bottom left output port. The sample, which had a concentration of $C = 10^{-3}$ M and a thickness of 50 μm, was placed on the stage. The fluorescence signal was recorded for various excitation powers, first while using the $\lambda = 543$ nm source and then with the $\lambda = 532$ nm laser. The results can be seen in Fig. 34, where a linear curve-fit was made for each set of data. Note that the measurements corresponding to the wavelength of $\lambda = 543$ nm are always higher than those for the wavelength $\lambda = 532$ nm.

From Fig. 34, the fitted value at an excitation power of 60 nW was chosen to compare the measurements taken with the different wavelengths. Figure 35 shows the difference in percentage between the fluorescence obtained with $\lambda = 543$ nm and $\lambda = 532$ nm, and it also compares it with the difference in absorption between these two wavelengths, obtained from Fig. 16 in Section 3.1.1. The fluorescence measured with the $\lambda = 543$ nm excitation source is 22% higher than what was obtained with the $\lambda = 532$ nm laser. For absorption, it is 31% higher for $\lambda = 543$ nm than for $\lambda = 532$ nm. Even though similar values were expected when comparing the absorption and emission, there is a decrease in the difference between the measured fluorescence for $\lambda = 532$ nm and for $\lambda = 543$ nm.

4.6 Pulsed and continuous excitation sources

In order to study the impact that the temporal distribution of the excitation beam had on the fluorescence emission, excitation with the $\lambda = 532$ nm cw laser and the $\lambda = 532$ nm pulsed laser was compared. As was seen in Section 2.3.6, even though the two lasers can

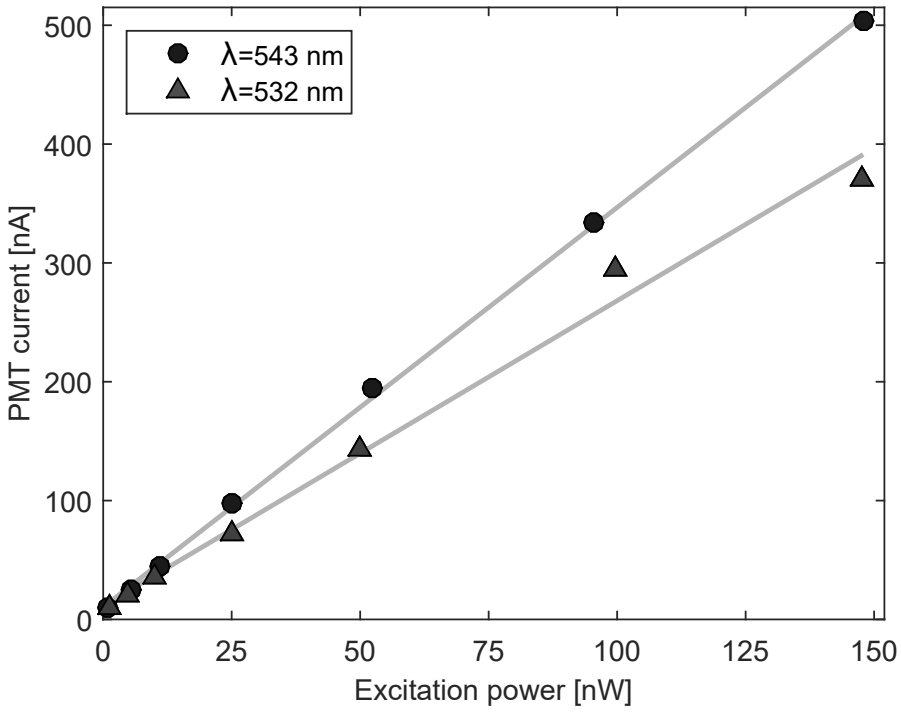

Figure 34: Fluorescence signal (PMT current) in relation to excitation power incident on the sample at different wavelengths of excitation. The sample used had a thickness of 50 μm and a concentration of C=10^{-3} M.

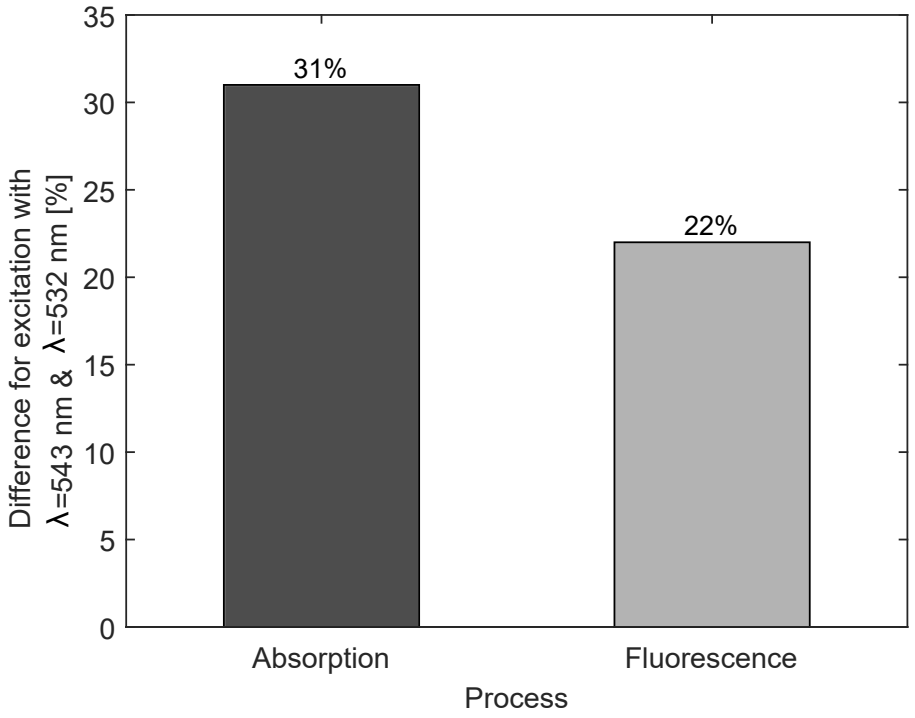

Figure 35: Difference in fluorescence emission, and difference in absorption when exciting with $\lambda = 532$ nm, as compared to using $\lambda = 543$ nm as the excitation wavelength.

supply the same average power, the peak power of the pulsed laser (assuming Δt=800 ps and f=20 kHz) is 62,500 times higher than the average power. Considering that the size of the illuminated area is the same regardless of the excitation source chosen, the intensity in the case of pulsed excitation can be high enough to saturate the Rhodamine B sample.

Samples of $C = 10^{-3}$, 10^{-4}, and 10^{-5} M , with a thickness of 50 μm were prepared. The PMT was placed at the *top* port, in the forward collection. Measurements of the fluorescence emission were recorded for each of the samples and both excitation sources, varying the average power at the microscope stage. The average power was changed to average intensity with Eq. (20) in Chapter 2. The results for the sample of concentration $C = 10^{-4}$ M are shown in Fig. 36. It can be seen that fluorescence with the cw excitation source maintains a linear relationship with the average intensity, while the pulsed source saturates the fluorescence emission.

The fluorescence intensity F for the one photon absorption case can be modeled

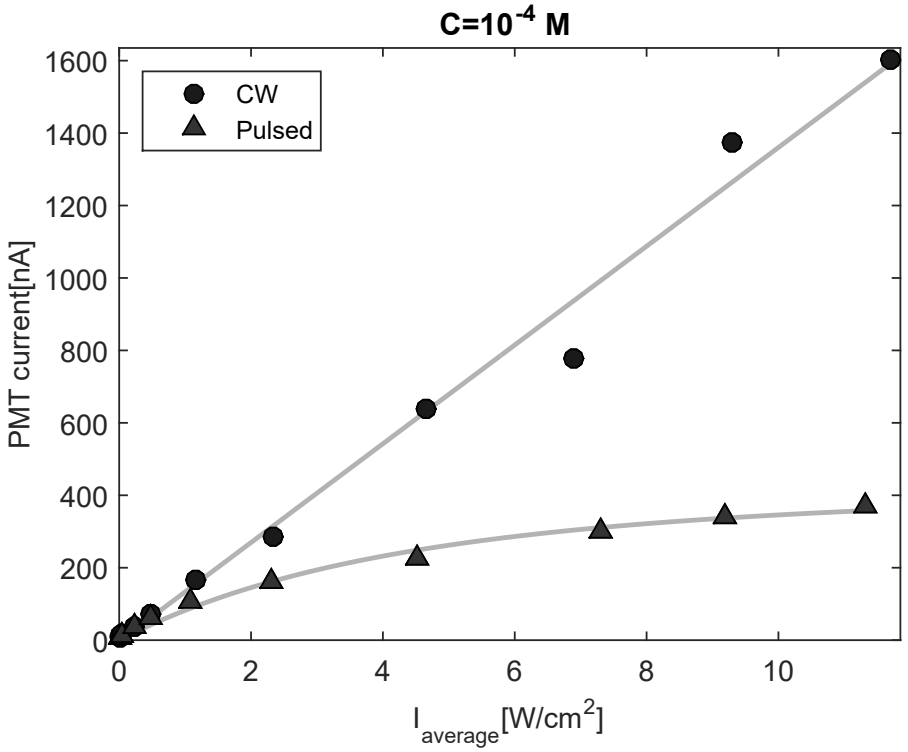

Figure 36: Fluorescence signal (PMT current) in relation to the average intensity at the microscope stage, for pulsed and continuous excitation with $\lambda = 532$ nm.

as [Wang *et al.*, 2004]

$$F = \phi\eta N_o \left[1 + \frac{1}{I/I_{sat}}\left(e^{-I/I_{sat}} - 1\right)\right], \tag{46}$$

where ϕ is the fluorescence collection efficiency of the measurement system, η is the fluorescence quantum efficiency of the sample, and N_o is the ground state population before the laser excitation. I_{sat} is the intensity at which saturation occurs and is given by

$$I_{sat} = \xi\frac{hc}{\sigma\Delta t\lambda}, \tag{47}$$

where Δt is the duration of the laser pulse, h is Planck's constant, c is the speed of light, λ is the wavelength of excitation, ξ is due to the spatial profile, and σ is the absorption cross section. The value of ξ for a Gaussian beam, can be approximated to ξ=1/2.

It can be seen from Eq. (47) that, knowing the characteristics of the excitation source, and if I_{sat} can be found, the value of the absorption cross section σ can be determined.

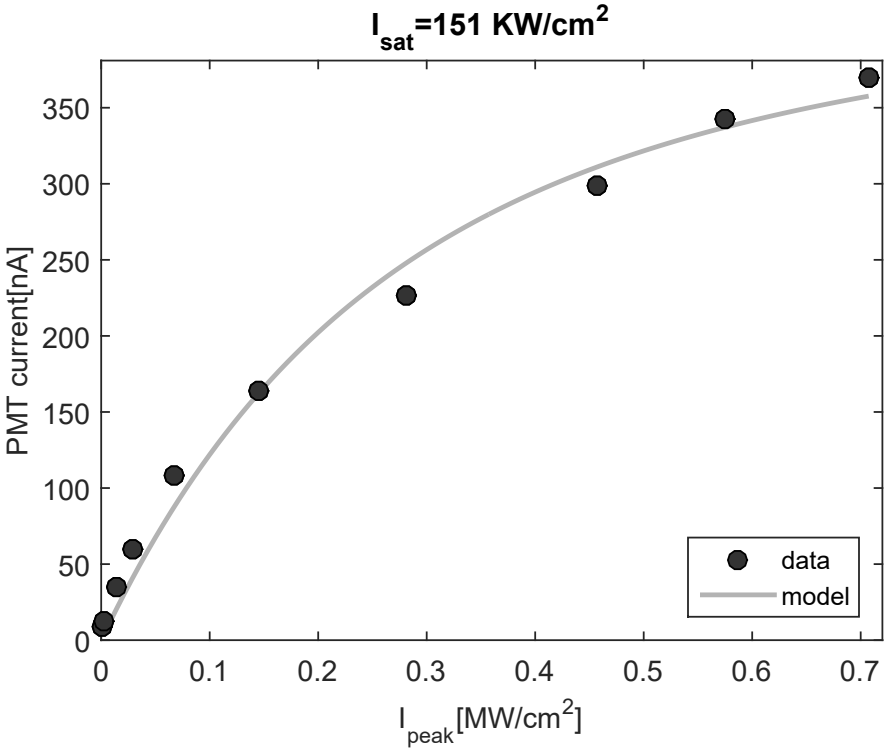

Figure 37: Fluorescence signal (PMT current) in relation to the peak intensity at the microscope stage, for pulsed excitation with $\lambda = 532$ nm.

By fitting the data taken for the pulsed excitation to the model given by Eq. (46), I_{sat} was calculated. Figure 37 shows how the model was fitted to the data for the sample with concentration $C = 10^{-3}$ M. Table 2 presents the saturation intensities found for the samples of different concentrations. The resulting calculated values for σ are shown in Table 3. The value of σ for Rhodamine B in MeOH with a concentration of $C = 10^{-3}$ M is reported to be 2.18×10^{-17} cm^2 at λ =435 nm [Srinivas *et al.*, 2003]. Even though a different wavelength was used, the values for σ were expected to be similar to what Srinivas $et\ al.$ obtained, but they are at least an order of magnitude higher. The absorption cross section obtained with the procedure described in Section 2.3.1 was $\sigma = 5.21 \times 10^{-17}$ cm^2 for a sample with $C = 10^{-3}$ M and 50 μm thickness.

Table 2: Saturation Intensity $\mathbf{I_{sat}}$ obtained by fitting the collected data from the samples of different concentrations to the model in Eq. (46).

C [M]	I_{sat} [KW/cm^2]
10^{-3}	231
10^{-4}	151
10^{-5}	396

Table 3: Absorption cross-section σ calculated using Eq. (47)**.**

C [M]	σ [m^2]
10^{-3}	1.01×10^{-15}
10^{-4}	1.55×10^{-15}
10^{-5}	5.90×10^{-16}

4.7 Geometry of the collection system

As has been stated before, the amount of emitted light that is able to reach the detector is determined by the optics of the collection system. To find the optical path best suited for collection, the different geometries constructed for the fluorescence microscopy system were compared.

Because the prepared sample could possibly deteriorate in a single day, care was taken when comparing the fluorescence collected with each of the three output ports. A measurement of the fluorescence was taken with the PMT positioned at the *bottom left* port. Without moving the microscope objective or the microscope stage sample holder position, the PMT was placed at the *back* port. Then, a measurement with the same sample and excitation power was taken, and the fluorescence emission signal recorded was compared. Another day, after finishing some measurements with the PMT at the *top* port, the same procedure as before was repeated with a new sample, but this time moving the PMT from the *top* port to the *bottom left* port. Figure 38 illustrates the difference in the fluorescence signal obtained by using the different collection ports. As can be seen from the figure, there was no difference in the fluorescence signal obtained from using the *back* or *bottom left* port. This means that the internal optics of the microscope objective are very efficient in transmitting the wavelengths in the fluorescence range. A higher fluorescence signal could be obtained when using the *top* port (4pi geometry) than when using the other ports corresponding to the epifluorescence configuration. The reason is that for collection with the 4pi geometry, there is no need for a dichroic filter, which has less than ideal transmission in this project. Something that should be said about using the *top* port is that this collection path proved to be considerably more difficult to align than any of the others, due to the use of the second microscope objective.

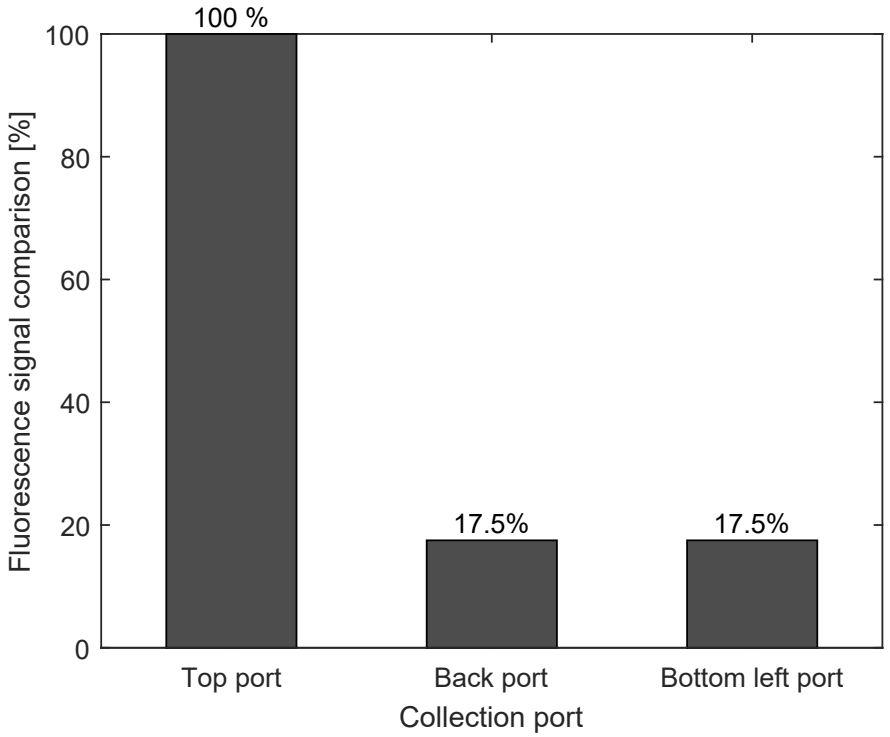

Figure 38: Comparison of the fluorescence signal (PMT current) obtained with different collection ports. The sample used had a thickness of 50 μm and a concentration of C=10^{-3} M.

4.8 Fluorescence emission peak position

In all of the experiments performed it was assumed that the fluorescence emission peak always fell within the collection window of the emission filter. This was reasonably based on the measurement of the emission spectrum of the sample with C=10^{-3} M. It was mentioned in the previous chapter that the peak position of the fluorescence emission may be influenced by a number of parameters, one of them being the concentration of the fluorophore. To determine if the peak position of the fluorescence emission changed significantly in the range of concentrations used, a spectrometer (Ocean Optics USB4000) was used to measure the emission spectrum of four samples with different concentrations, when excited with $\lambda = 543$ nm. The fluorescence emission peak was slightly shifted towards shorter wavelengths as the concentration decreased.

As seen in the Jablonski diagram (Fig. 4, Chapter 2), after excitation occurs, the internal conversion process brings the excited molecule to the lowest vibrational level of the first excited state. Thus, regardless of the vibrational level that the fluorophore was excited

to, emission always occurs from the same vibrational level of S_1. For this reason, the fluorescence emission spectrum is independent of the excitation wavelength, and using the different excitation sources should not affect the peak position. To verify this assumption, the spectrum of a sample with $C = 10^{-3}$ M and 50 μm thickness was measured for the three excitation sources used. Table 4 lists the fluorescence emission peak wavelength for each of the excitation sources. There was no difference between the $\lambda = 532$ nm pulsed and continuous sources, so it can be said that the amount of photons illuminating the fluorophore sample has no impact on the peak position of fluorescence emission. There is however difference between the $\lambda = 543$ and the $\lambda = 532$ nm sources, with the first source yielding a spectrum shifted 2 nm towards longer wavelengths in comparison with the second.

Table 4: Fluorescence emission peak wavelength $\lambda_{\mathbf{peak}}$ for different excitation sources.

Excitation Source	λ_{peak} [nm]
cw, $\lambda = 543$ nm	586.0
cw, $\lambda = 532$ nm	584.0
pulsed, $\lambda = 532$ nm	584.0

4.9 Excitation with low power

After seeing that higher fluorescence signals could be obtained when using the forward collection path, it was interesting to determine how low could the excitation power be reduced to in the system, while still producing an observable signal. The PMT was placed at the *top* port, and a sample of 50 μm thickness and concentration C=10^{-3} M was prepared. The sample was placed in the stage, and the focusing position was adjusted to z=-25 μm. The fluorescence signal was recorded for four different excitation powers, in the range from 0.05 to 1.12 nW. Figure 39 shows the data obtained. Because the dark current background of the PMT was measured to be 9 nA, only measurements above this threshold are valid. Even though excitation with 0.12 nW yielded an average fluorescence signal of 11.4 nA, the error bars where too close to the background value to claim it as significantly observable. It can be said then, that by carefully selecting the parameters studied in previous sections, with the most contributing factors being the collection geometry and the concentration, an observable signal with an excitation power of around 0.5 nW can be obtained. This is an important result that can be used when working with

low levels of light, whether to minimize photodamage to the sample or due to limitations of the excitation source.

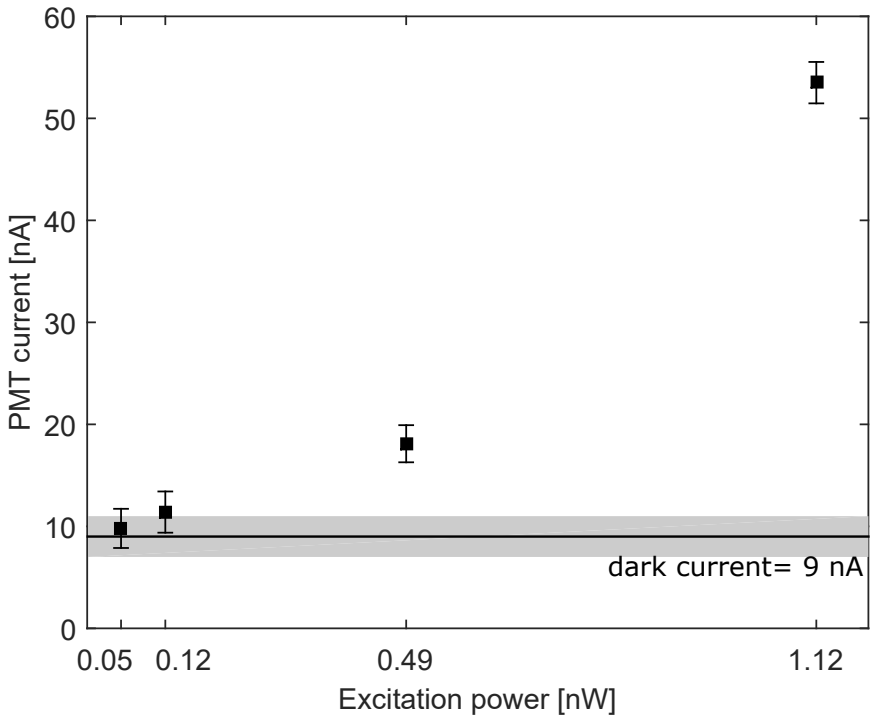

Figure 39: Fluorescence signal for excitation power less than 2 nW.

Chapter 5. Conclusions

The purpose of this work has been to investigate the theoretical and experimental parameters involved in fluorescence induced in liquid fluorophore samples at a microscopic scale. The fluorophore used was Rhodamine B with methanol as the solvent. Before performing any experiment, a bibliographical research of the fundamentals of fluorescence, the parameters involved, and the characteristics of the fluorophore used was done. The spatial distribution of the intensity near focus for a low N.A. microscope objective illuminated with a truncated Gaussian beam was simulated using the approach of Horvath and Bor (2003). Then, a fluorescence microscopy system with two possible geometries was designed and constructed. It allowed for parameters related to the sample, such as concentration and thickness, to be investigated. It also permitted the study of parameters related to the system, such as the wavelength of excitation, focusing position of the microscope objective, use of continuous or pulsed excitation, and geometry of the collection system. In the following five paragraphs, the results obtained are briefly summarized.

A CMOS camera was used to obtain images of the excitation beam and the resulting fluorescence in the homogeneous sample. A broadening of 10 times the size of the excitation beam spot was observed for the fluorescence in the case of a sample with 100 μm thickness and concentration $C = 10^{-3}$ M. A 50 μm sample of the same concentration had less broadening, which leads to the hypothesis that it is influenced by the sample thickness.

For the rest of the experiments, a photomultiplier was used as a detector. A relatively small difference in the fluorescence signal was found between samples of different thickness, so it was not a critical parameter. Deviations from the expected value in the measurements of the fluorescence signal when only varying one aspect of the experiment are a reminder that some of the fluorescence parameters, such as the quantum yield and concentration, cannot be considered independent from one another. Still, the highest concentration $C = 10^{-3}$ M provided the highest fluorescence signals. Regarding the excitation focusing position in the sample, one-photon excitation fluorescence occurs throughout the entire sample thickness. For the collection system built, even when the focused beam waist is not located within the Rhodamine B solution part of the sample, a fluorescence

signal could be obtained. Nevertheless, a higher signal could be achieved by placing the beam waist within it. At least for the low numerical aperture objective used, the position within the solution did not have a strong effect.

As for the wavelength of excitation, fluorescence signals with excitation wavelengths $\lambda = 543$ nm and $\lambda = 532$ nm were compared. The difference between the two fluorescence obtained in the two cases can be credited to the fluorophore absorption's wavelength dependence, with the absorption peak occurring at $\lambda = 543$ nm. Even though there was more fluorescence than expected for $\lambda = 532$ nm, as there were no significant differences on peak emission wavelength. This means it cannot be attributed to more efficient transmittance of the optical elements or a higher sensitivity of the detector to the fluorescence wavelengths for this excitation.

A comparison of fluorescence for pulsed and continuous excitation sources of the same wavelength was also performed and, while the cw laser showed a linear dependence on excitation power, the pulsed laser was found to saturate the fluorescence signal. The value of intensity saturation was obtained from the pulsed excitation data, which allowed for determination of the absorption cross-section of the fluorophore.

The construction of the fluorescence microscopy system allowed for the use of two different collection configurations. These configurations were 4pi geometry and epifluorescence. The advantages and disadvantages that each geometry offered depended on the equipment available and on the alignment of each experimental arrangement. Due to the efficiency of the dichroic filter used, the 4pi geometry proved to collect a higher amount of fluorescence than the epifluorescence configuration. By using the 4pi geometry and carefully selecting the parameters of the system and of the sample, an observable signal with excitation power as low as 0.5 nW could be obtained.

In future work, a more effective collection system could be constructed by using the 4pi technique of collection through both microscope objectives. Thus, the collection efficiency of the system could be doubled. Regarding the theoretical calculations, it would be interesting to determine the intensity distribution near the focal plane for lenses of higher N.A., and to also consider the effects of the aberrations of the objectives.

To summarize, a study of fluorescence microscopy that has allowed for the acquisition of significant fluorescence signals with low excitation power has been presented. This work represents the beginning of the efforts in the Quantum Optics Laboratory of CICESE to utilize fluorophore samples with non-classical sources of entangled photon pairs.

List of Bibliographical References

Abramowitz, M. (2003). *Microscope basics and beyond*. Olympus America Inc., Melville, NY. pp. 42.

Berland, K. (2001). *Basics of Fluorescence*. Springer New York. p. 5-19.

Bindhu, C. V. and Harilal, S. S. (2001). Effect of the excitation source on the quantum-yield measurements of rhodamine B laser dye studied using thermal-lens technique. *Analytical Sciences*, **17**: 141–144.

Boni, L. D., Franzen, P. L., Gonçalves, P. J., Borissevitch, I. E., Misoguti, L., Mendonça, C. R., and Zilio, S. C. (2011). Pulse train fluorescence technique for measuring triplet state dynamics. *Opt. Express*, **19**(11): 10813–10823.

Born, M. and Wolf, E. (1999). *Principles of Optics (4th ed.)*. Cambridge University Press. pp. 985.

Duarte, F. J., Hillman, L. W., and Liao, P. F. (1990). *Dye Laser Principles with Applications*. Academic Press Inc., San Diego CA. pp. 293.

Fang, W., Shan, X., Li, Z., Sun, C., Li, Z., Men, Z., and Fan, L. (2012). Stimulated resonance Raman scattering of Rhodamine B. *Optik - International Journal for Light and Electron Optics*, **123**: 1845–1846.

Goodman, J. (1996). *Introduction to Fourier Optics (3rd ed.)*. Mc Graw Hill, US. pp. 441.

Hecht, E. (2002). *Optics (4th ed.)*. Addison Wesley. pp. 680.

Hell, S. and Wichmann, J. (1994). Comparison of different theories for focusing through a plane interface. *Optics letters*, **19**(11): 780–782.

Horvath, Z. L. and Bor, Z. (2003). Focusing of truncated Gaussian beams. *Optics Communications*, **222**: 51–68.

Ishii, S., Mizoi, T., Kawano, K., Cay, O., Thomas, P., Nachman, A., Ford, R., Shoji, Y., Kruskal, J., Steele, Glenn, J., and Jessup, J. (1996). Implantation of human colorectal carcinoma cells in the liver studied by in vivo fluorescence videomicroscopy. *Clinical & Experimental Metastasis*, **14**(2): 153–164.

Islam, M. M., Chakraborty, M., Pandya, P., Masum, A. A., Gupta, N., and Mukhopadhyay, S. (2013). Binding of DNA with Rhodamine B: Spectroscopic and molecular modeling studies. *Dyes and Pigments*, **99**(2): 412 – 422.

Jensen, E. (2012). Types of imaging, Part 2: An overview of fluorescence microscopy,. *The Anatomical Record*, **295**: 1621–1627.

Khosrofian, J. and Garetz, B. (1983). Measurement of a Gaussian laser beam diameter through the direct inversion of knife-edge data. *Appl. Opt.*, **22**: 3406–3410.

Lakowicz, J. R. (2007). *Principles of fluorescence spectroscopy (3rd ed.)*. Springer US. pp. 954.

Sagoo, S. K. (2011). *Intrinsic properties of Rhodamine B and Fluorescein gas-phase ions studied using laser-induced fluorescence and photodissociation in a quadrupole ion trap mass spectometer*. M.S. Thesis. University of Toronto. 75 p.

Saleh, B. and Teich, M. (2007). *Fundamentals of Photonics (2nd ed.)*. New Jersey, Wiley & Sons. p. 74-100.

Sigma-Aldrich (2015). Rhodamine b for fluorescence. Retrieved from: www.sigmaaldrich.com/catalog/product/sigma/83689.

Sluder, G. and Wolf, D. (2003). Digital microscopy:a second edition of video microscopy. *Methods in Cell Biology*, **72**: 1–523.

Spring, K. and Davidson, M. (2015a). Depth of field and depth of focus. Retrieved from: www.microscopyu.com/articles/formulas/formulasfielddepth.html.

Spring, K. and Davidson, M. (2015b). Introduction to fluorescence microsopy. Retrieved from: http://www.microscopyu.com/articles/fluorescence/fluorescenceintro.html.

Spring, K., Russ, J., Turchetta, R., Parry-Hill, M., Long, J., Fellers, J., and Davidson, M. (2015). Digital imaging in optical microscopy. Retrieved from: http://www.olympusmicro.com/primer/digitalimaging/index.html.

Srinivas, N. K. M. N., Rao, S. V., and Rao, D. N. (2003). Saturable and reverse saturable absorption of rhodamine b in methanol and water. *J. Opt. Soc. Am. B*, **20**(12): 2470–2479.

Valeur, B. (2001). *Molecular fluorescence: Principles and applications,*. New Jersey, Wiley & Sons. pp. 381.

Wang, Y., Tai, O., Wang, C., and Jen, K. (2004). One-, two-, and three-photon absorption induced fluorescence of a novel chromophore in chloroform solution. *J. Chem. Phys.*, **121**: 7901–7907.

Wiersma, S., Török, P., Visser, T., and Varga, P. (1997). Comparison of different theories for focusing through a plane interface. *J. Opt. Soc. Am. A*, **14**: 1482–1490.

Xu, C. and Webb, W. W. (1996). Measurement of two-photon excitation cross sections of molecular fluorophores with data from 690 to 1050 nm. *J. Opt. Soc. Am. B*, **13**(3): 481–491.

Xu, C. and Webb, W. W. (2002). *Topics in Fluorescence Spectroscopy*. Springer US. pp. 544.

ZEISS-Campus (2015). Introduction to fluorescence microsopy,. Retrieved from: http://zeiss-campus.magnet.fsu.edu/articles/basics/fluorescence.html.